

1 **Earth's earliest global glaciation? Carbonate geochemistry and geochronology of the**
2 **Polisarka Sedimentary Formation, Kola Peninsula, Russia**

3

4 A.T. Brasier^{1,6*}, A.P. Martin²⁺, V.A. Melezhik^{3,4}, A.R. Prave⁵, D.J. Condon², A.E. Fallick⁶ and
5 FAR-DEEP Scientists

6

7 1 Faculty of Earth and Life Sciences, Vrije Universiteit Amsterdam, De Boelelaan 1085, 1081HV
8 Amsterdam

9 2 NERC Isotope Geosciences Laboratory, British Geological Survey, Environmental Science
10 Centre, Keyworth, UK. NG12 5GG

11 3 Geological Survey of Norway, Postboks 6315 Sluppen, NO-7491 Trondheim, Norway

12 4 Centre for Geobiology, University of Bergen, Postboks 7803, NO-5020 Bergen, Norway

13 5 Department of Earth and Environmental Sciences, University of St Andrews, St Andrews KY16
14 9AL, Scotland, UK

15 6 Scottish Universities Environmental Research Centre, Rankine Avenue, East Kilbride, Scotland.
16 G75 0QF

17

18 *corresponding author (a.t.brasier@vu.nl)

19 + present address: GNS Science, Private Bag 1930, Dunedin, New Zealand

20

21 Research highlights:

22 ICDP FAR-DEEP Hole 3A targeted Palaeoproterozoic diamictites of the Polisarka Sedimentary
23 Formation of Russian Fennoscandia ► Zircon U-Pb dating of a tuff above the diamictites yielded
24 an interpreted minimum age of 2434 Ma for the diamictites ► This new U-Pb age constrains the
25 onset of the Palaeoproterozoic glaciation in Fennoscandia to between ca. 2430 and ca. 2440 Ma ►

26 carbonate $\delta^{13}\text{C}$ analyses of carbonate rocks below the diamictites revealed two excursions to ca. -
27 5‰ ► the origins of these excursions are carefully considered

28

29 **Abstract**

30 As part of the International Continental Scientific Drilling Program's Fennoscandian Arctic Russia
31 – Drilling Early Earth Project (ICDP FAR-DEEP), Palaeoproterozoic diamictic and associated
32 rocks were targeted and recovered in Hole 3A on the Kola Peninsula of NW Russia. In addition to
33 the diamictites, carbonate sedimentary rocks and volcanic ash layers (all metamorphosed to
34 greenschist grade) were encountered. Sedimentology and geochemistry suggest deposition of the
35 diamictites in an open-marine aragonite-precipitating environment. Sampling of the core and of
36 outcrops from the same geographical area yielded a number of zircons for analyses, the majority of
37 which were inherited. However a tuff at 20.01 m core depth yielded zircons dated at 2434 ± 1.2 Ma
38 (± 6.6 Myr including decay constant uncertainties) that we interpret as a magmatic age. These data,
39 combined with dates from underlying intrusions, indicate deposition of the Polisarka Sedimentary
40 Formation diamictites and underlying carbonates during an interval of time from ca. 2430 to 2440
41 Ma. The carbonate rocks, which likely originally included aragonitic limestones, were deposited
42 mostly in a deep-water setting (i.e. at least below storm wave base) and occur below the diamictite.
43 They record two inorganic carbon $\delta^{13}\text{C}$ excursions, from values of ca. 0‰ to minima of ca. -5.4‰,
44 as the contact with the overlying diamictite is approached. The older excursion occurs about 9 m
45 below the base of the diamictic units and the younger one at 1m below. Throughout that interval,
46 Mg/Ca ratios correlate strongly with $\delta^{13}\text{C}$ ($n = 38, r = 0.85$), and combined with petrographic
47 observations, this indicates that the first (stratigraphically lower) excursion was modified by
48 secondary alteration and the second is recorded in resedimented dolostone clasts. It is tempting to
49 speculate that these dolostone clasts were deposited in penecontemporaneous shallow-marine
50 waters, and that their low $\delta^{13}\text{C}$ values might reflect input of oxidised atmospheric methane to the
51 ocean surface (and therefore the cause of the glaciation); the dolostones were subsequently

52 resedimented into the deeper marine settings. However this must be left as a hypothesis to be tested
53 when further age-constrained contemporaneous pre-glacial carbonate sections are found.

54

55 Keywords:

56 Huronian-age glaciation; carbon isotopes; carbonate rocks; Palaeoproterozoic; Great Oxidation
57 Event

58

59 **Introduction**

60 During the purported global glaciation episode(s) of the Palaeoproterozoic, ice extended from the
61 poles to low latitudes at least once (e.g. Evans et al., 1997; Mertanen et al., 1999; Melezhik, 2006;
62 Melezhik et al., 2013a; Hoffman, 2013). These early glaciations may have been as significant for
63 biological and geological evolution as the ‘Snowball Earth’ episodes in the Neoproterozoic, a
64 billion years later. Robust geochemical testing of proposed causes for severe climatic deterioration
65 in the Palaeoproterozoic has been hindered by lack of suitable rock types in immediately pre-glacial
66 sections.

67

68 Varied explanations for initiation of glaciation have included atmospheric CO₂ (greenhouse gas)
69 drawdown resulting from enhanced chemical weathering of silicate rocks because of collisional
70 tectonics (Young, 1991), rifting at low latitudes (e.g. Evans, 2003), and a combination of tectonic
71 and environmental factors (Melezhik, 2006). These models implicitly require lengthy (million-year
72 timescale) durations as they involve processes operating at rates of the geological rock cycle, and
73 all permit repeat episodes of global freezing, as observed in the rock record. Another potential
74 driver to consider is catastrophic and rapid oxidation of Earth’s proposed early methane atmosphere
75 (e.g. Kasting et al., 1983; Pavlov et al., 2000; Kopp et al., 2005; Papineau et al., 2005; 2007). Here,
76 the warming effect of a methane-rich atmosphere might have counteracted the relative weakness of
77 the young Sun and a methane atmosphere was invoked to explain the relative lack of evidence for

78 glaciation until the Palaeoproterozoic (Pavlov et al., 2000; see also corrections by Haqq-Misra et
79 al., 2008). This state-of-affairs ended when atmospheric free oxygen first became widespread ca.
80 2.4 billion years ago (e.g. Pavlov et al., 2000; Kopp et al., 2005; Kasting, 2005; Melezhik, 2006;
81 Haqq-Misra et al., 2008; Guo et al., 2009), the ‘Great Oxidation Event’ (GOE). Photochemical
82 dissociation of ozone in the newly oxic atmosphere (with less free H₂) would have given rise to free
83 OH[•] radicals. These, in turn, could have reacted with methane to produce CH₃ + H₂O, as well as a
84 series of short-lived organic molecules (Ravishankara, 1988), and, finally, bicarbonate ions. It has
85 been estimated that the GOE would have shortened the lifetime of methane in the atmosphere from
86 10⁵ to ~10¹ years (as found at present; Pavlov et al., 2003; Kasting, 2005). Although it now seems
87 that methane alone would not have been a sufficiently strong greenhouse gas to keep the early Earth
88 ice-free (e.g. Haqq-Misra et al., 2008), the latter authors concluded that loss of methane from the
89 atmosphere was still a likely trigger for glaciations around 2.4 billion years ago. The methane
90 oxidation hypothesis is testable because it implies a one-off, unrepeatable rapid transfer of a vast
91 quantity of ¹³C-depleted carbon from the atmosphere to the surface oceans, thereby initiating the
92 first Palaeoproterozoic glaciation. This likely would have been recorded in contemporaneous
93 marine carbonate rocks, which is why Palaeoproterozoic carbonate rocks below diamictites recently
94 discovered in Fennoscandian Russia are important. These were found in International Continental
95 Drilling Program (ICDP) Fennoscandian Arctic Russia – Drilling Early Earth Project (FAR-DEEP)
96 Hole 3A which targeted the Polisarka Sedimentary Formation of the Imandra-Varzuga Belt (Fig. 1).
97
98 Evidence for Palaeoproterozoic glaciation in the Fennoscandian region includes diamictites and
99 dropstones of the Urkkavaara Formation (Sariolian group, Marmo and Ojakangas (1984)). There
100 are known dropstones in sediments with varve-like laminations in the Polisarka Sedimentary
101 Formation (Imandra-Varzuga Greenstone Belt; Melezhik et al., 2013b) and its stratigraphic
102 equivalents in the Shambozero and Lekhta Greenstone Belts (cf. Negruța, 1984). None of these
103 naturally exposed Fennoscandian sections are known to include a carbonate unit below the

104 diamictite, so the discovery of such rocks in ICDP FAR-DEEP Hole 3A was serendipitous. Stable
105 isotopic analyses of these carbonate rocks are reported here, with the aim of illuminating the cause
106 of the glaciation. In addition, volcanic ash beds have been sampled for U-Pb dating of zircons to
107 constrain the age of the diamictite-containing Polisarka Sedimentary Formation, thereby aiding
108 global correlations and geologic context.

109

110 **Geological setting**

111 ICDP FAR-DEEP Hole 3A was drilled in the Imandra-Varzuga Greenstone Belt at latitude
112 67.4862N, longitude 34.5404E, between the 7th and 14th September 2007, to a total depth of 254.5
113 m (see Fig. 1). The target was the Palaeoproterozoic Polisarka Sedimentary Formation (Fig. 2),
114 known from outcrop to contain diamictites (Fig. 3f) that could correlate with the Huronian
115 diamictites of North America (Melezhik, 2013). Depths given in this manuscript are in metres
116 composite depth (MCD).

117

118 The diamictite-containing Polisarka Sedimentary Formation sits unconformably on the Seidorechka
119 Volcanic and Sedimentary formations, both of which overly the Kuksha and Purnach formations
120 (Fig. 2). The Kuksha Volcanic Formation lies unconformably on the Monchegorsk layered gabbro-
121 norite pluton (Chashchin et al., 2008), and the Kuksha Sedimentary Formation seals eroded and
122 faulted surfaces of the pluton (Melezhik, 2013; Melezhik et al. 2013a). Zircons from the Monche
123 Pluton were radio-isotopically dated at 2504.4 ± 1.5 Ma (ID-TIMS $^{207}\text{Pb}/^{206}\text{Pb}$ weighted mean date;
124 Amelin et al., 1995). In the mid- to upper-Seidorechka Formation, baddeleyite grains in a
125 subvolcanic unit yield a 2442.2 ± 1.7 Ma age (ID-TIMS upper intercept date; Amelin et al., 1995).
126 This unit is spatially and temporally associated with an intrusion (the Imandra lopolith) dated by U-
127 Pb ID-TIMS at 2441 ± 1.6 Ma (ID-TIMS $^{207}\text{Pb}/^{206}\text{Pb}$ weighted mean date; Amelin et al., 1995).

128 In the western part of the Imandra-Varzuga Greenstone Belt, the Avarench locality is comprised of
129 a komatiitic basalt – andesite – dacite – rhyolite association that is considered the lithostratigraphic

130 equivalent of Strelna Group rocks, including the Kuksha and Seidorechka Formations. Zircons
131 extracted from two samples of plagioclase and quartz dacitic metaporphyrites yield an age at $2429 \pm$
132 6.6 Ma (U-Pb zircon SHRIMP date; Vrevsky et al., 2010). This dated unit is considered to be the
133 litho- and chrono-stratigraphic equivalent of the Seidorechka Volcanic Formation (e.g., Melezhik,
134 2013). The c. 2504 Ma age of the Monche Pluton is the maximum age for the Imandra-Varzuga belt
135 succession, and provides one age constraint to the Polisarka Sedimentary Formation. However, if
136 the interpretation of Amelin et al. (1995) that the subvolcanic (c. 2442 Ma) unit is a ‘feeder’ to the
137 Seidorechka Volcanic Formation is correct, then the age of the spatially associated Imandra
138 Lopolith (slightly younger than 2442Ma, at ca. 2441 Ma) can be taken as a maximum age for the
139 Polisarka Sedimentary Formation.

140

141 *ICDP FAR-DEEP Hole 3A: stratigraphic and preservational context of the carbonates*

142 The Polisarka Sedimentary Formation in ICDP FAR-DEEP Hole 3A is sandwiched between
143 rhyodacites of the underlying Seidorechka Volcanic Formation and mafic komatiites of the
144 overlying Polisarka Volcanic Formation. It was informally divided by Melezhik et al. (2013b) into a
145 lower carbonate-rich Limestone member and an upper siliciclastic Greywacke-diamictite member.
146 The contact between these members lies at around 123.8 m depth. The first thick diamictite bed
147 occurs at around 114 m (Fig. 2). Three smaller diamictite units have been documented in the
148 Limestone member. The first out-sized clast associated with deformed underlying laminae occurs at
149 183.2m but its origin as a potential dropstone is tempered by the fact that variably developed
150 tectonic shearing is present in ICDP FAR-DEEP Hole 3A. Clasts and dropstones (Fig. 3a; 3g) are
151 commonly tectonically flattened or exhibit sigmoidal morphologies, with their long axes parallel to
152 bedding and shearing (Fig. 3a). In the Limestone member, millimetre-scale laminations comprising
153 laterally discontinuous layers of carbonate alternating with layers of siltstone might reflect an
154 original sedimentary texture (Fig. 3b; Melezhik et al., 2013b), but bedding-parallel shearing can
155 generate transposed bedding resulting in a metamorphic-related ‘pseudo-lamination’. This

156 greenschist facies metamorphism complicates the interpretation of depositional environments here,
157 but sedimentary features can be distinguished in low-strain zones.

158

159 On a broad scale, Melezhik et al. (2013b) suggested that fine compositional laminae and lack of
160 traction-bedded structures indicate a relatively deep-water setting (below effective storm and
161 fairweather wave base) for the Limestone member (Fig. 2). They suggested that exotic and faceted
162 diamictite clasts that in places pierce compositional layering indicate a glacio-marine origin for the
163 Greywacke-diamictite member. The transition from the Limestone member to the overlying
164 Greywacke-diamictite member is one of siliciclastic upward coarsening over several metres, and the
165 contact itself is marked by a sharp-based medium to coarse-grained laminated arkosic sandstone.

166 These relationships are consistent with glacio-eustatic sea-level fall, with the arkosic bed
167 representing a consequent base level incision and basinward facies shift. It is difficult to assess the
168 water depth in which the glacial diamictites were deposited, but we assume that they were deposited
169 in at least similar and likely shallower settings than the carbonate rocks.

170

171 Melezhik et al. (2013b) briefly described several igneous bodies encountered in the Limestone
172 member (Fig. 2). These include a thin alkaline ultramafic body (225.15 to 225.97 m) that is best
173 interpreted as a dyke belonging to the Palaeozoic alkaline province of the Kola Peninsula; 0.2 to 4m
174 thick mafic bodies that have been interpreted as Palaeoproterozoic lava flows (212 to 189 m); and a
175 44 m thick massive ultramafic peridotite (175.68 to 131.17 m). Diagnostic features that would allow
176 the latter to be ascribed as either intrusive or extrusive seem to be lacking. Igneous bodies including
177 komatiites are also encountered above the diamictite sediments (Fig. 2).

178

179

180 **Methodology: stable isotopes and elemental geochemistry**

181 Methods used in the sampling and analyses of rock samples for their stable isotopic and elemental
182 compositions are given in detail in the Supplementary Information.

183

184 **Methodology: U-Pb geochronology**

185 Targeted for chronology were 14 samples from drill core 3A; one field specimen containing
186 dropstones from the Polisarka Sedimentary Formation; one field sample from the Ahmalahti
187 Formation that stratigraphically overlies the Polisarka Sedimentary Formation; and three samples
188 from the Seidorechka Volcanic Formation that stratigraphically underlies the Polisarka Sedimentary
189 Formation. For U-Pb dating an analytical approach combining laser ablation inductively coupled
190 plasma mass spectrometry (LA-ICPMS) with subsequent isotope dilution thermal ionisation mass
191 spectrometry (ID-TIMS) of grains of interest (i.e., likely younger than the existing maximum age
192 constraint) was employed. Further details are given in Supplementary Information.

193

194 **Results**

195

196 *Sedimentary rock petrography*

197 Sedimentary rocks of the Limestone member (Melezhik et al., 2013b) include finely laminated
198 ‘limestone and siltstone couplets’ (Fig. 3). Some of the carbonate layers are continuous across the
199 core width (Fig. 3b), while others form discontinuous lenses (see Figs. 3c and 3d; also Melezhik et
200 al., 2013b). The sedimentary protoliths of these layered carbonate-siliciclastic rocks were likely
201 carbonate and quartz-rich siltstones, now metamorphosed to marbles with interlocking crystal
202 fabrics. Some marbles are relatively pure carbonate rocks, like those found at 128.35 m (Fig. 4a),
203 while others include layers of quartz and talc found at 182.44 m and 201.14 m (Figs. 4b and 4c).

204

205 Layered carbonate-siliciclastic rocks both below and above the peridotite body (Fig. 2) commonly
206 contain laminae of a soft metallic grey mineral with a blue sheen in hand-specimen. In thin-section

207 this mineral shows pleiochromism from light brown to colourless (Fig. 4d), with birefringence to 2nd
208 order red. The mineral is therefore deduced to be talc, and this concurs with bulk rock XRD
209 analyses (Table S1 in supplementary information). In thin-sections, several crenulated talc layers
210 are cross-cut (replaced) by euhedral rhombs of dolomite (Fig. 4d). Talc-replacement carbonate
211 rhombs (shown as they appear in the core in Fig. 3e) are found in abundance in other sections of the
212 stratigraphy, particularly within the serpentinised peridotite body between 175.68 m and 131.17 m
213 (Fig. 4e). Petrographic examination reveals that komatiites at 81.69 m are also carbonatised and
214 serpentinised (Fig. 4f).

215

216 Distinctly different in appearance to the secondary dolomite rhombs are dusty-looking and more
217 rounded carbonate clasts conclusively identified only around 126.97 m depth (Fig. 5). These clasts
218 are found in at least four 3 cm-thick beds separated by foliated thin carbonate layers. Staining with
219 Alizarin Red S revealed that the clasts are dolomitic, and the sheared carbonate layers are
220 dominantly calcitic. These rocks lack talc, but do contain laths of white mica aligned parallel
221 layering (Fig. 5) and interpreted as the metamorphic product of clay minerals. This mica is most
222 prominent in calcitic foliated layers (these layers lack quartz) and also occurs with small quartz
223 crystals around the margins of dolostone clasts (but is absent in the clasts). The mineralogy deduced
224 from petrography is consistent with bulk rock XRD analysis (Table S1; quartz, calcite, dolomite,
225 muscovite).

226

227 Veins and veinlets comprised of quartz and carbonate, some of which are ptlygmatically folded, are
228 found in several places (Figs. 3d, 4b and 7). Their presence raises the prospect that circulating
229 meteoric, burial or metamorphic fluids might have altered carbonate stable isotope compositions.
230 Following acquisition of bulk rock stable isotope data (Fig. 6), carbonate rocks around a quartz vein
231 that occupies approximately 20cm of the core at ca. 125 m depth (Figs. 2 and 7), and a 1 cm thick
232 quartz veinlet at ca. 126.85 m, were targeted for sampling, to assess whether carbonate stable

233 isotopic compositions were affected by vein-associated fluids. Carbonate veins were also analysed
234 for their stable isotopic composition and include those sampled from above and below, as well as
235 within, the peridotite body. The final phase of carbonate present is as mm-thick brown weathering
236 alteration rims around diamictite clasts; these, too, were sampled for stable isotopic analyses using a
237 hand-drill.

238

239 *Elemental chemistry results*

240 Elemental concentrations of powdered samples measured by XRF give data applicable to the whole
241 rock, whereas the ICP-AES data should relate more specifically to the carbonate component.

242 Magnesium concentrations (measured by ICP-AES) of the carbonates range from 1410 to 97600
243 ppm, and Mg/Ca molar ratios up to a maximum of 47% Mg (vs 53% Ca). The carbonates are
244 therefore limestones to calcitic dolostones. Elemental analyses of bulk rock powders have not
245 revealed any stoichiometric dolostones in these cores. On the basis of available elemental data, the
246 main intervals of dolostone in FAR-DEEP Hole 3A are from 221 to 225 m; immediately above the
247 peridotite at 130.94m; and from ~124 to 127.4 m. However some samples have ‘out of sequence’
248 Mg/Ca values if the trend from ~124 to 127.4 m is interpreted as purely depth- and time- related
249 (Fig. 6). Importantly, Mg/Ca molar ratio correlates very strongly with $\delta^{13}\text{C}$ over the interval of the
250 carbon isotope excursions (Fig. 7): the lowest $\delta^{13}\text{C}$ values are undoubtedly from Mg-rich carbonates
251 ($n = 38$, $r = 0.85$).

252

253 Cr and Ni concentrations of acetic-acid soluble (‘carbonate’) components (measured by ICP-AES)
254 also correlate very strongly with $\delta^{13}\text{C}$ between 130.82 and 124.33 m depth (see Table S2 in
255 supplementary information). Chromium and nickel concentrations of the first carbonate sample
256 above the peridotite are very high (38 and 12 ppm, respectively). Whole-rock Cr and Ni
257 concentrations (measured by XRF) do not show the strong correlation with carbonate $\delta^{13}\text{C}$ between
258 130.82 and 124.33 m .

259

260 Strontium concentrations (ICP-AES) range from 13 to 1180 ppm. Manganese concentrations (ICP-
261 AES) range from 8 to 3980 ppm. Mn/Sr molar ratios (ICP-AES) range from 0.33 to 23 with the
262 highest ratio from any sample below the peridotite (Fig. 8) being 8.1. Mn/Sr (ICP-AES) molar
263 ratios > 9 are found at 130.94 m (the first carbonate sample above the peridotite) and in all
264 measured bulk rock samples from ~127.8 m upwards (Fig. 8). The maximum Mn/Sr ratio of 23 at
265 126.01 m is exceptional. Whole-rock Mn/Sr ratios (measured by XRF) are mostly lower (< 5, with
266 a maximum measured value of 8.7). Overall Mn/Sr trends in the XRF bulk rock data are similar to
267 those found in the ICP-AES 'carbonate' data.

268

269 *Carbonate stable isotope results*

270 Measured bulk carbonate rock $\delta^{13}\text{C}$ values in FAR-DEEP Hole 3A range from +0.9 to -5.4‰
271 (VPDB). The minimum $\delta^{13}\text{C}$ value from the 44 'hand-drilled' carbonate powders was -7.5‰, with a
272 maximum of +0.6‰. Below 177 m depth, almost all $\delta^{13}\text{C}$ values fall in the range 0 ± 1 ‰. Above
273 178 m, at least two $\delta^{13}\text{C}$ excursions to minima of around -6‰ are seen (Fig. 6). The first begins at
274 ~177.5 m, with $\delta^{13}\text{C}$ falling to -2.7‰ from a starting position 2 m below the base of the peridotite.
275 Carbon isotopic compositions of secondary dolostone crystal growths within the peridotite were
276 measured at -6.4‰ (sample from 135 m), while veins in the peridotite are less negative at the base
277 of the body (-4.0‰; 150.49 m) than at the top (-6.6‰; 132.8 m). All other secondary carbonates
278 obtained from within the peridotitic section gave $\delta^{13}\text{C}$ compositions within this range.

279

280 The first 'bulk' carbonate rock sample above the peridotite (at 130.94 m) has low $\delta^{13}\text{C}$ of -5.4‰,
281 and this was confirmed by a value of -5.8‰ from a sample of the same brown discoloured
282 carbonate taken from 131.1 m (Fig. 6). The carbon isotope trend is towards 0‰ in the overlying
283 carbonate rocks, reaching 0‰ at 129.78 m before declining to a nadir of -5.9‰ in dolostones at

284 125.60 m. There is a recovery to -1.9‰, although there is considerable scatter (Fig. 6). A final
285 negative swing to -7.4‰ at 122.32 m is based on only one data point.

286

287 Carbonate rocks that appear least likely to be altered on the basis of their petrography and distance
288 from potential fluid conduits such as veins gave the least negative $\delta^{13}\text{C}$ compositions, mostly near
289 0‰, *except* for the dolostone clasts (those of 126.97 m, shown in Fig. 5), plus one diamictite clast
290 and one sample of ‘marble’ from 126.87 m. The latter comes from very close to the preserved
291 dolostone clasts. The ‘clastic’ dolostone grains from 126.97 m (Fig. 5) themselves exhibit
292 significantly more negative $\delta^{13}\text{C}$ values (-4.9 to -5.0‰) than the intervening calcite-containing
293 sheared layers (-3.0 to -4.0‰).

294

295 All veins or likely secondary carbonate rocks below the peridotite body gave ‘normal’ or ‘near
296 normal’ $\delta^{13}\text{C}$ compositions, similar to the surrounding carbonate rock. The majority (but not quite
297 all) veins and metamorphosed sedimentary carbonate rocks judged to be in proximity to veins
298 above the peridotite gave negative $\delta^{13}\text{C}$ values. In one case (129.97 m), a carbonate sample from
299 within a few millimetres of a vein gave $\delta^{13}\text{C}$ of -4.3‰ while carbonate rock 15 cm above the vein
300 gave a value of -0.7‰. Brown-coloured (dolomitic?) alteration rims around clasts in the diamictite
301 all gave very low $\delta^{13}\text{C}$ values, typically around -7‰.

302

303 The oxygen isotope data are all isotopically light. Bulk samples gave a $\delta^{18}\text{O}$ range from -16.2 to -
304 23.8‰ (VPDB), while ‘hand drilled’ sample data range from -14.7 to -25.0‰. Except for the two
305 extreme values all other data from the hand-drilled samples lie between -16.4 and -22.3‰. It should
306 be recalled that none of these oxygen isotope data are corrected for their Mg content.

307

308 A cross-plot of $\delta^{18}\text{O}$ vs $\delta^{13}\text{C}$ (Fig. 9) reveals some significant trends. First it is clear that the
309 majority of all samples have $\delta^{18}\text{O}$ values between -20 and -22‰. Some of the more Mg-rich

310 carbonates have slightly elevated $\delta^{18}\text{O}$ (Fig. 6), particularly those near the base of the hole
311 (affecting carbonates with $\delta^{13}\text{C}$ ca. 0‰) and not correcting for Mg content (by up to -1.4‰) could
312 partly explain this. However the population of very low $\delta^{13}\text{C}$, Mg-rich carbonates exhibits $\delta^{18}\text{O}$
313 compositions comparable to the majority of the ‘normal’ $\delta^{13}\text{C}$ carbonates, or perhaps slightly more
314 negative than the modal value (particularly if a dolomite correction were applied). Most intriguing
315 are a sub-set of ‘calcites’ (as determined by Alizarin Red S staining) with elevated $\delta^{18}\text{O}$ (up to -
316 16.4‰) and $\delta^{13}\text{C}$ from -3.0 to -4.0‰. These seem to form a mixing line trend with ‘dolomites’
317 from the same sample (126.97m) that have low $\delta^{13}\text{C}$ and low to modal $\delta^{18}\text{O}$ compositions (Fig. 9).
318 One sample of secondary quartz extracted from the ICDP FAR-DEEP Hole 3A cores at 223.30 m
319 has $\delta^{18}\text{O}_{\text{sil}}$ of 11.4 ‰ (VSMOW) most likely indicating a relatively high temperature of
320 precipitation.

321

322 *U-Pb geochronology: results and interpretation*

323 The samples targeted for chronology are summarised in Table S3 in the supplementary information,
324 and sample depths for ICDP FAR-DEEP Hole 3A are shown on Fig. 10. Of the 19 studied samples,
325 only eight yielded zircons. A total of 218 zircons were obtained, and all were subjected to LA-
326 ICPMS screening. Relative probability plots of $^{207}\text{Pb}/^{206}\text{Pb}$ ages from LA-ICP-MS for all zircon-
327 bearing samples are shown in Fig. 10 (excluding Sample 3A 207.85 m which yielded only two
328 Archaean dates). The maximum age of the Polisarka Sedimentary Formation (ca. 2441 Ma) is
329 shown on each plot (Fig. 10). Samples 3A 22.90m and Ru1310 show nine grains whose $^{207}\text{Pb}/^{206}\text{Pb}$
330 ages are younger than 2441 Ma. When each of the nine grains was picked and further analysed by
331 U-Pb ID-TIMS they were shown to have Archaean ages > 2600 Ma. This discrepancy can be
332 attributed to the larger errors associated with the LA-ICP-MS method, masking Pb-loss in the nine
333 grains. Only zircons from an andesitic fine tuff, Sample 3A 20.01 m from ICDP FAR-DEEP Hole
334 3A (Fig. 11), were shown to have ages < 2441 Ma (and therefore of potential geochronological use
335 here) when analysed by U-Pb ID-TIMS. The results of dating of all sixteen zircon crystals obtained

336 from Sample 3A 20.01m (Fig. S1 in supplementary information) are shown in Table 1. Of these
337 sixteen crystals, ten yielded $^{207}\text{Pb}/^{206}\text{Pb}$ dates at ca. 2700 Ma. These grains have a prismatic nature,
338 reflecting their xenocrystic incorporation of older material. The remaining six ID-TIMS analyses
339 yielded $^{207}\text{Pb}/^{206}\text{Pb}$ dates from ca. 2410 to 2436 Ma (Fig. S1 and Table 1). Four of these grains (z2,
340 z7, z8 and z9) are discordant and display correlations between $^{207}\text{Pb}/^{206}\text{Pb}$ age and magnitude of
341 discordance (Table 1), suggesting non-zero age Pb-loss. As such, these four $^{207}\text{Pb}/^{206}\text{Pb}$ dates are
342 likely to be inaccurate. The two remaining analyses (z11 and z12) are concordant (Fig. 12), giving
343 overlapping $^{207}\text{Pb}/^{206}\text{Pb}$ dates of 2432.8 ± 2.1 and 2435.9 ± 1.5 Ma and an error weighted mean
344 $^{207}\text{Pb}/^{206}\text{Pb}$ date of 2434.8 ± 1.2 Ma (assuming age equivalence of the two dated zircons and using a
345 value of 137.88 for $^{238}\text{U}/^{235}\text{U}$ for consistency with older studies; see supplementary information).
346 Incorporation of the uncertainties in $\lambda^{235}\text{U}$ and $\lambda^{238}\text{U}$ (Jaffey et al., 1971), required only when
347 comparing $^{207}\text{Pb}/^{206}\text{Pb}$ dates with those from other decay schemes like Re-Os, increases the
348 uncertainty to 6.6 Myr.

349

350 Given the potential global significance of the U-Pb date obtained, the context and petrography of
351 the sample is described here. Rock sample 3A 20.01 m was intersected around 100 m above the top
352 of the carbonate-bearing interval (and ca. 80 m above the diamictites), between 20.01 and 20.30 m
353 in ICDP FAR-DEEP Hole 3A (Fig. 2). In hand specimen (Fig. 11a), altered and compacted pumice
354 fragments (0.5 to 1 mm) have a common alignment, giving the rock a discontinuous, streaky
355 appearance. Lithic fragments (0.25 mm) and crystals (0.1 mm) are also present. In thin section (Fig.
356 11b), the altered pumice clasts (constituting 5% volume of the rock) are uniformly aligned with a
357 eutaxitic texture, suggesting welding or in-situ diagenetic compaction. Fragments observed include
358 volcanic quartz (3% volume) with small embayments and straight extinction, and less commonly
359 plagioclase (1% volume). Rare lithic fragments, composed of plagioclase and pyroxene, are found
360 in a fine groundmass of feldspar, quartz, and opaque minerals. Weak chlorite alteration is evident in
361 the groundmass. This rock is best classified as an andesitic fine tuff (White and Houghton, 2006) on

362 the basis of the presence of quartz and feldspar; a light to moderate colour index; the presence of
363 pumice and fragments of crystals and (rare) lithics; and a fine groundmass. The clast type, clast
364 morphology, and grain size range indicate that this fine tuff has not experienced interim storage
365 prior to lithification. The morphologies of the zircon crystals (30 – 70 μm) recovered varied, with
366 some large prismatic grains (albeit visibly metamict) with aspect ratios up to 8, and some smaller
367 faceted grains with aspect ratios of 1.5 to 2. However there is a distinct morphological sub-
368 population of prismatic crystals and crystal fragments with medial melt inclusion ‘tunnel’ traces: a
369 feature that typifies volcanic zircon (z1, z2, z7 z8 and z11 in Fig. S1) and is characteristic of the ca.
370 2435 Ma population. Although post-depositional re-working is likely to have been restricted, we
371 must also consider whether the ca. 2435 Ma zircons were inherited into the magma prior to
372 eruption, and thus reflect a maximum age. Whilst we cannot categorically rule this out, making the
373 age strictly a maximum age, however we note that (1) the dated zircons are distinctly younger than
374 the known ca. 2441 Ma dates from underlying intrusions; and (2) numerous levels were sampled for
375 zircon (fig. 10) and whilst a number of samples did contain inherited zircons they were all >2.5 Ga;
376 the ca. 2435 population only occurs in Sample 3A 20.01, a distinct andesitic fine tuff. Therefore,
377 based upon the concordant U-Pb systematics, the morphology of the dated zircons, and their
378 geological context, the $^{207}\text{Pb}/^{206}\text{Pb}$ date of $2434.8 \pm 1.2/6.6$ Ma (analytical/total uncertainty) is
379 interpreted to approximate the age of the andesitic fine tuff and inferentially the age of the sampled
380 stratigraphic level.

381

382 **Discussion**

383

384 *U-Pb chronology and chronological correlations*

385 Zircon grains from an andesitic fine tuff (Sample 3A 20.01m) yield a $^{207}\text{Pb}/^{206}\text{Pb}$ age at $2434.8 \pm$
386 1.2 Ma; this is interpreted as an eruption age, contemporaneous with sedimentation at this
387 stratigraphic level. The age of the Polisarka Sedimentary Formation below 20.01 m in ICDP FAR-

388 DEEP Hole 3A is therefore constrained between the inferred age of the underlying Seidorechka
389 Volcanic Formation at 2441 ± 1.6 Ma, and the newly derived age of Sample 3A 20.01 m at 2434.8
390 ± 1.2 Ma. This age range encompasses deposition of the carbonate rocks and the diamictite units in
391 ICDP FAR-DEEP Hole 3A (Fig. 6). The SHRIMP zircon date of 2429 ± 6.6 Ma (Vrevsky et al.,
392 2010) from units in western part of the Imandra-Varzuga Greenstone Belt that have been inferred to
393 represent the top of the Seidorechka Volcanic Formation are broadly consistent with the ID-TIMS
394 age from the eastern sector, the slightly younger age perhaps being biased by non-zero age Pb-loss
395 and/or analytical calibration.

396

397 These age constraints on deposition of the Polisarka Sedimentary Formation diamictite allow
398 confident comparison with diamictite units deposited elsewhere. Palaeoproterozoic diamictite
399 sections crop out in the Great Lakes region of North America, including the Huronian Supergroup
400 in Canada and the Marquette Range Supergroup in the USA. Palaeoproterozoic diamictites are also
401 known from the Transvaal Supergroup of South Africa, and the Meteorite Bore Member of Western
402 Australia. Whilst the sedimentology of these sections is relatively well understood, the age
403 constraints on these sections remain relatively poor.

404

405 There are three diamictite-bearing formations in the Huronian Supergroup (from oldest to
406 youngest): Gowganda, Bruce, and Ramsay Lake. These three formations are underlain by the
407 Thessalon Formation where zircons in the Copper Cliff rhyolite member have been dated at $2450 \pm$
408 25 Ma (ID-TIMS; Krogh et al., 1984); providing a maximum age constraint to diamictite
409 deposition. The three diamictite-bearing formations are cross-cut by the Nipissing intrusions, dated
410 at ca. 2200 Ma (for example 2217 ± 9 Ma; ID-TIMS on baddeleyite and rutile fractions; Corfu and
411 Andrews, 1986). This date is therefore a minimum age constraint to diamictite deposition in the
412 Huronian Supergroup sections. It has been noted that the diamictite-bearing Gowganda Formation
413 is cross-cut by dykes with peperitic margins (Young et al, 2001), suggesting the youngest of the

414 Huronian Supergroup diamictites may have been deposited at ca. 2200 Ma (if the cross-cutting
415 dykes are equivalent to the Nipissing intrusions) or older. The Polisarka Sedimentary Formation
416 diamictite could therefore be equivalent in age to any of the Huronian Supergroup diamictites.

417

418 The Marquette Range Supergroup, in the Menominee and Iron River – Crystal Falls Ranges area,
419 includes the diamictite-bearing Fern Creek Formation that is in turn overlain by the Sturgeon
420 Quartzite. The youngest detrital zircons in this latter formation yield a 2306 ± 9 Ma date (SHRIMP;
421 Vallini et al., 2006), providing a minimum age constraint to deposition of the Fern Creek Formation
422 diamictite. There is no maximum age. The temporal relationship between the Fern Creek Formation
423 diamictite and the Polisarka Sedimentary Formation diamictite remains to be clarified.

424

425 In the Marquette Range Supergroup (Marquette Range area) the diamictite-bearing Enchantment
426 Lake Formation has yielded detrital zircons whose youngest age is 2317 ± 6 Ma (SHRIMP; Vallini
427 et al., 2006), providing a maximum age constraint to the formation's deposition. Furthermore,
428 hydrothermal xenotime has been dated in the same formation at 2133 ± 11 Ma (SHRIMP; Vallini et
429 al., 2006), giving a minimum age constraint for deposition. The Polisarka Sedimentary Formation
430 diamictite was therefore deposited earlier than the Enchantment Lake Formation diamictite.

431

432 In South Africa the diamictite-bearing Duitschland and Boshhoek Formations crop out in the
433 Transvaal basin. The Rooihoogte Formation is commonly considered the lithostratigraphic
434 equivalent to the Duitschland Formation (Hannah et al., 2004) and contains authigenic pyrite that
435 has been dated by the Re-Os method at 2316 ± 7 Ma (Hannah et al., 2004); this is a maximum age
436 constraint to deposition of the Boshhoek Formation diamictite. Rocks several units above the
437 Boshhoek Formation are intruded by the Bushveld Complex, where zircons have yielded a 2054 ± 2
438 Ma date (SHRIMP; Scoates and Friedman, 2008), considered a suitable minimum age constraint to
439 the Boshhoek Formation diamictite. The Polisarka Sedimentary Formation diamictite was therefore

440 deposited before the Boshhoek Formation diamictite. The 2316 ± 7 Ma date for the Rooihogte
441 Formation is also a minimum age constraint to diamictite deposition in the Duitschland Formation.
442 A concordant U-Pb SHRIMP age on a zircon in the upper part of the Duitschland Formation yields
443 a $^{207}\text{Pb}/^{206}\text{Pb}$ age at 2424 ± 12 Ma that is a maximum age to this formation (Dorland, 2004). Several
444 igneous units beneath the Duitschland Formation have been dated, with a zircon age at 2480 ± 6 Ma
445 (SHRIMP; Nelson et al., 1999) on the Penge Formation also providing a maximum age constraint to
446 the diamictite-bearing Duitschland Formation. Contemporaneous deposition of the Duitschland and
447 Polisarka Sedimentary formation diamictite units is thus permissible, given the current age
448 constraints on the African section.

449

450 The diamictite-bearing Meteorite Bore Member crops out in Australia's Hammersley Basin.
451 Underlying the Meteorite Bore Member by several units, zircons in a lava flow of the Woongarra
452 Rhyolite Formation have yielded a 2449 ± 3 Ma date (ID-TIMS; Barley et al., 1997). This is a
453 maximum age constraint to diamictite deposition in the Hammersley Basin. Baddeleyite grains from
454 a mafic sill that cross-cuts the Meteorite Bore Member have been dated at 2208 ± 10 Ma (SHRIMP
455 Müller et al., 2005) and are a minimum age constraint to deposition of the diamictite. The diamictite
456 deposition ages of the Meteorite Bore Member and the Polisarka Sedimentary Formation overlap,
457 which is not surprising, given that the Australian diamictite could have been deposited at any time
458 during a ca. 240 Myr interval.

459

460 The Polisarka glacial deposits could be equivalent to any of the three Huronian Supergroup
461 diamictite-bearing strata, but the loss of mass-independent fractionation of sulphur isotopes (MIF)
462 recorded in Canada, Africa and Fennoscandia may provide further independent constraints. The
463 permanent disappearance of sulphur MIF occurs between the first and second diamictite in South
464 Africa (Guo et al., 2009) and Canada (Papineau et al., 2007), suggesting that one can correlate the
465 lower Duitschland with the Ramsay Lake, the upper Duitschland with the Bruce, and the

466 Makganyene-Timeball Hill with the Gowganda diamictites (e.g., Melezhik et al. 2013a). If correct,
467 then the presence in Fennoscandia of both MIF and mass-dependent fractionation in the pre-
468 Huronian rocks (Reuschel et al., 2009), and a pronounced mass-dependent fractionation in the
469 Huronian interval (Melezhik et al., 2013b), could reflect that the Polisarka glacial deposits correlate
470 either with the Gowganda/Makganyene-Timeball Hill or with the upper Bruce/Duitschland
471 diamictites. In any case the Polisarka Sedimentary Formation diamictites were certainly deposited
472 prior to the Enchantment Lake (Marquette Range Supergroup) and Boshhoek (Transvaal
473 Supergroup) diamictite-bearing units. We suggest here that the age of the diamictite-bearing
474 Polisarka Sedimentary Formation is constrained to between 2434.8 ± 1.2 Ma (tuff in the Polisarka
475 Volcanic Formation) and 2441 ± 1.6 Ma (subvolvanic intrusions in the Seidorchka Formation),
476 indicating this represents an early (perhaps the earliest) Palaeoproterozoic glaciation.

477

478 *Carbonate geochemistry*

479

480 *Sr abundances*

481 All analysed carbonate rock samples from the Polisarka Sedimentary Formation contain high Sr
482 contents, ranging between 560 and 1030 ppm (767 ppm on average, $n = 14$). Several limestones
483 have Sr concentrations higher than 800 ppm with a few samples containing 900–1030 ppm.
484 Inorganic aragonites and calcites in equilibrium with modern seawater contain approximately 9000
485 and 1000 ppm Sr, respectively (Veizer, 1983), and Sr content in seawater has likely remained near-
486 constant through time (Steuber and Veizer, 2002). Hence the values measured from the Polisarka
487 carbonates are close to equilibrium concentrations of modern marine calcites (Veizer, 1983;
488 Schlanger, 1988). However, the recrystallisation textures strongly argue for post-depositional
489 alteration of most of the analysed samples, hence for a significant Sr loss from these rocks. It has
490 been shown that each recrystallisation step in an open system reduces Sr content in the newly
491 formed calcite by a factor of 10, and in dolomite by a factor 20 (Veizer, 1983; Banner, 1995). Since

492 diagenetic and metamorphic alteration rarely takes place in an open system, the loss of Sr is
493 commonly less. Taking into account the strong petrographic evidence for recrystallisation
494 throughout the hole, the samples with 900–1000 ppm Sr are likely products of a precursor phase
495 with a very high initial Sr content, hence much of the carbonate was likely originally deposited as
496 aragonite.

497

498 *Oxygen isotopes*

499 The evidence for deformation fabrics throughout the core and likely Sr loss from the carbonate
500 rocks do not require that every geochemical proxy has been entirely overprinted, because the
501 requisite water/rock ratios differ for each tracer (Banner, 1995). However, the invariably low (for
502 Palaeoproterozoic marine carbonates; e.g. Schidlowski et al., 1975) oxygen isotopic compositions
503 of the ICDP FAR-DEEP Hole 3A carbonates are intriguing. Veizer et al. (1992) reported carbonate
504 $\delta^{18}\text{O}$ values between -5 and -10‰ (VPDB) from the Transvaal Supergroup (South Africa) and Duck
505 Creek Dolomite (Western Australia), but from -13 to -18‰ (VPDB) in the Bruce Member
506 limestones of North America. They suggested that such low values might either reflect a non-
507 marine depositional environment for the Bruce Member, or a contribution from high latitude or
508 altitude glacial melt waters. In the case of the Polisarka Sedimentary Formation data, the
509 interpretation of these $\delta^{18}\text{O}$ values (mostly between -19 and -22‰ vs VPDB) must be left open, but
510 noting that the carbonate rocks have recrystallised in the presence of a hot fluid, such that their $\delta^{18}\text{O}$
511 values may no longer be representative of the original carbonate oxygen isotopic composition.
512 Quartz extracted from a carbonate layer at a depth of 223.30m with $\delta^{18}\text{O}_{\text{sil}}$ of 11.4‰ VSMOW is
513 also consistent with silica precipitation from a hot fluid (ca. 300 °C, for fluid $\delta^{18}\text{O}$ of 4‰ VSMOW;
514 Matsuhisa et al., 1979). A second overprinting of carbonate oxygen isotopic compositions by a late
515 stage meteoric or shallow burial fluid that preferentially affected calcites relative to dolomites
516 would provide an explanation for the sub-set of ‘calcites’ around 126 m depth with elevated $\delta^{18}\text{O}$

517 (up to -16.4‰) and $\delta^{13}\text{C}$ from -3.0 to -4.0‰. The possible oxygen isotope mixing line trend in this
518 sample (Fig. 9) would then result from mixing between ‘calcite’ and ‘dolomite’ end-members.

519

520 *Robustness of the carbonate carbon isotope signal*

521 The carbonate carbon isotopes are here of special interest because of the possibility they could
522 reflect marine dissolved inorganic carbon (DIC) prior to one of the early Palaeoproterozoic
523 glaciations, potentially aiding understanding of its cause. Interpreting the carbon isotopes in this
524 way first requires an assessment of the extent of secondary alteration and whether there might still
525 be a primary signal retrievable from the data.

526

527 The carbonate rocks are all to varying extents recrystallised, but recrystallisation alone is not
528 necessarily an indicator that the carbon isotopes of these carbonates are reset: note that carbonates
529 with ‘normal’ $\delta^{13}\text{C}$ are as affected by this pervasive recrystallisation as those containing the low
530 $\delta^{13}\text{C}$ signal. Because interaction between carbonates and meteoric fluids commonly increases Mn
531 concentrations and decreases Sr concentrations of the rocks, marine carbonates with Mn/Sr ratios
532 <3 (e.g. Derry et al., 1992) or <10 (Kaufman and Knoll, 1995) are commonly believed to have
533 retained original seawater DIC signals in their $\delta^{13}\text{C}$. Carbonate rocks here would all meet the Mn/Sr
534 <10 criterion (mostly being between about 3 and 5) except for the first sample immediately above
535 the peridotite, and all samples from above ca. 127.8 m (Fig. 8). Using the ICP-AES Mn/Sr ratio
536 data, the $\delta^{13}\text{C}$ of all samples associated with the second and most prominent $\delta^{13}\text{C}$ excursion could
537 be considered suspect. However, these ICP-AES data are from ‘bulk carbonate’ so do not
538 discriminate between calcite of clear secondary origin and the primary dolostone clasts. The Mn/Sr
539 values cannot be reliably used as an indicator of carbonate carbon isotope alteration in these mixed
540 dolomite – calcite samples that contain the second prominent negative carbon isotope excursion.

541 The XRF elemental data reflect only the whole rock (i.e. including silicate) composition. The Mn/Sr

542 molar ratios calculated from these XRF data are all < 10 , although the XRF dataset is more limited
543 than the ICP-AES dataset here.

544

545 Correlation between carbonate oxygen isotopes and carbon isotopes can also be indicative of post-
546 depositional alteration in cases where the oxygen isotopes have been altered. A complicating factor
547 to using this approach here is the variable mineralogy of the carbonate rock samples. Correlation
548 between carbonate $\delta^{13}\text{C}$ and $\delta^{18}\text{O}$ (Fig. 9) is best explained as the result of mixing between low
549 $\delta^{13}\text{C}$, low $\delta^{18}\text{O}$ dolostone and high $\delta^{13}\text{C}$, high $\delta^{18}\text{O}$ secondary calcite end-members. This approach
550 cannot therefore be used to distinguish primary from altered carbon isotope signals in this case. It is
551 however encouraging that the dolostone clasts and secondary calcite yield different values,
552 testifying that the carbonate carbon isotopes of ICDP FAR-DEEP Hole 3A have not been entirely
553 overprinted by any late-stage secondary fluid interaction.

554

555

556 *Carbon isotopes and magnesium abundances*

557 Strong correlation between increasing Mg/Ca ratios and decreasing $\delta^{13}\text{C}$ values in some sections of
558 ICDP FAR-DEEP Hole 3A (Fig. 6) means the origin(s) of the Mg/Ca trend may bear directly on the
559 interpretation of the carbon isotope data. The elevated Mg in samples from 221 to 225 m is due to
560 the presence of dolomite, although the reasons for its occurrence in this section of the core are
561 unclear. The petrography of these sheared and recrystallised rocks is very similar to those of
562 surrounding carbonate rocks with more calcitic compositions. Elevated Mg/Ca values are also seen
563 from ~124 to 127.4 m, and there are several possible explanations for this. First is the possibility
564 that the Mg derives from the adjacent ultramafic igneous rocks, perhaps during and following
565 metamorphism at greenschist facies (ca. 300°C). This seems an attractive explanation for samples
566 taken from brown stained and chlorite-rich sections immediately above the peridotite at 130.94 m.
567 While the $\delta^{13}\text{C}$ is very low in this sample (as it is in dolomite crystals that have replaced talc in the

568 peridotite below), elemental concentrations of Ni and Cr are very high, perhaps due to alteration by
569 fluids circulating between the (Mg, Ni and Cr-rich) peridotite and overlying carbonate. However it
570 is worth noting that serpentinisation and carbonatisation of peridotite consume and do not produce
571 CO₂, although of course CO₂ flux may accompany emplacement. The isotopically negative carbon
572 isotope signatures of these carbonates (including the dolomite crystals replacing talc) must here be
573 explained either by carbon from Palaeoproterozoic sea- or meteoric water, or perhaps decarbonation
574 reactions during metamorphism, or by local alteration involving externally sourced (perhaps
575 magmatic and/or hydrothermal) fluids.

576

577 Analysis of the prominent and smoothly curved excursion to low $\delta^{13}\text{C}$ that reaches a nadir around
578 125.60 m depth shows alteration by fluids interacting with the peridotite to be untenable. This
579 second excursion occurs away from obvious bedding or structural contacts and entirely within a
580 sedimentary carbonate section (Fig. 7), separated from the peridotite body by several metres of
581 carbonate rock with $\delta^{13}\text{C}$ of 0 to -1‰. There are no obvious features consistent with preferential
582 channelling of diagenetic fluids through the low $\delta^{13}\text{C}$ section except some quartz veins (see Fig.
583 12). But their siliceous composition implies hot basinal fluids were silica-rich and carbon-poor, so
584 unlikely to dramatically alter $\delta^{13}\text{C}_{\text{carb}}$.

585

586 Above 130 m depth the Mg/Ca values are consistent with calcitic carbonate compositions, except
587 for between ca. 124 and 127.4 m. Here the petrography suggests the presence of (primary)
588 dolomitic clasts with some secondary calcite (Fig. 5). It seems most likely that these dolostone
589 clasts were resedimented from shallower settings. It is possible that they were derived from erosion
590 of a much older carbonate platform, although older formations in this area are not known to contain
591 any likely dolostone sources. Hence it seems reasonable to suggest that the clastic dolostone likely
592 formed in shallow waters penecontemporaneously with deeper water calcites, in the run-up to the
593 Huronian glaciation. If correct, then the carbon isotopic composition of the allochthonous dolostone

594 clasts records the pre-Huronian shallow-water marine DIC, while the deeper-water DIC is recorded
595 by the majority of the (calcitic) carbonates in ICDP FAR-DEEP Hole 3A. Correlation between
596 Mg/Ca and $\delta^{13}\text{C}$ in the carbonates between ~124 and 127.4 m (Fig. 6) could then be explained by
597 mixing lines between deep water calcites with near-zero per mil $\delta^{13}\text{C}$ and shallow-water-derived,
598 isotopically light dolostone clasts. There are clearly several plausible reasons for why the dolostone
599 clasts exhibit low $\delta^{13}\text{C}$ values. One speculative hypothesis that we cannot conclusively rule out is
600 oxidation of isotopically light methane, and its incorporation into shallow dolomite-precipitating
601 waters.

602

603 **Conclusions**

- 604 1. The new U-Pb data reported here likely constrain the onset of the Palaeoproterozoic
605 glaciation recorded by the Polisarka Diamictite to a narrow time-window between ca. 2441
606 ± 1.6 Ma and 2434.8 ± 1.2 Ma. Considering constraints from other cratons, this glacial
607 deposit likely records one of the earliest Palaeoproterozoic glaciations, and perhaps the
608 earliest.
- 609 2. The ICDP FAR-DEEP Hole 3A carbonate carbon isotope data imply Palaeoproterozoic
610 seawater DIC shallow-to-deep trends in which lighter values characterise the shallower
611 water settings. We speculate that this reflects atmospheric methane oxidation. However this
612 interpretation must be viewed with circumspection in that the carbonate carbon isotope
613 profile includes resedimented dolostone clasts that we infer were derived from
614 contemporaneous shallower settings. Further, at least some of the carbon isotope values
615 have been affected by post-depositional processes. Resolving these issues will likely require
616 discovery of another section containing pre-glacial carbonates of the same age, either in
617 Fennoscandia or elsewhere.

618 3. Geochemical data, such as the high Sr-content in the Polisarka limestones, strongly suggest
619 aragonite precipitation from penecontemporaneous marine waters. A Polisarka "aragonite
620 sea" might have been associated with an elevated Mg content in contemporaneous seawater.

621

622 **Acknowledgements**

623 ATB and AM were supported by NERC grant NE/G00398X/1 to AEF, ARP and DJC. VAM is
624 supported by NFR grant 191530/V30 (projects 331000 and 802795).

625

626 **References**

627 Amelin, Y. V., Heaman, L. M., and Semenov, V. S., 1995. U-Pb geochronology of layered mafic
628 intrusions in the eastern Baltic Shield: implications for the timing and duration of
629 Paleoproterozoic continental rifting. *Precambrian Res* 75, 31-46.

630 Banner, J.L., 1995. Application of the Trace-Element and Isotope Geochemistry of Strontium to
631 Studies of Carbonate Diagenesis. *Sedimentology* 42, 805-824.

632 Barley, M. E., Pickard, A. L. and Sylvester, P. J., 1997. Emplacement of a large igneous
633 province as a possible cause of banded iron formation 2.45 billion years ago. *Nature*, 385:
634 55-58.

635 Bekker, A., Holland, H.D., Wang, P.-L., Rumble III, D., Stein, H.J., Hannah, J.L., Coetzee, L.L.,
636 and Beukes, N.J., 2004, Dating the rise of atmospheric oxygen: *Nature*, v. 427, p. 117-120.

637 Bots, P., Benning, L.G., Rickaby, R.E.M., S. Shaw, S., 2011. The role of SO₄ in the switch from
638 calcite to aragonite seas. *Geology*, v. 39, p. 331-334.

639 Chashchin, V.V., Bayanova, T.B., Levkovich, N.V., 2008, Volcanoplutonic association of the
640 early-stage evolution of the Imandra–Varzuga rift zone, Kola Peninsula, Russia: geological,
641 petrogeochemical, and isotope-geochronological data. *Petrology*, v. 16, p. 279–298 (in
642 Russian).

643 Corfu, F., and Andrews, A.J., 1986, A U-Pb age for mineralized Nipissing diabase,

- 644 Gowganda, Ontario: Canadian Journal of Earth Sciences, v. 23, p. 107–109.
- 645 Derry, L.A., Kaufman, A.J., Jacobsen, S.B., 1992. Sedimentary Cycling and Environmental-
646 Change in the Late Proterozoic - Evidence from Stable and Radiogenic Isotopes.
647 *Geochimica et Cosmochimica Acta* 56, 1317-1329.
- 648 Dorland, D.H., 2004. Provenance ages and timing of sedimentation of selected Neoproterozoic and
649 Paleoproterozoic successions on the Kaapvaal Craton. PhD thesis, University of
650 Johannesburg, 326 p.
- 651 Evans, D.A., Beukes, N.J., and Kirschvink, J.L., 1997, Low-latitude glaciation in the
652 Palaeoproterozoic era: *Nature*, v. 386, p. 262-266.
- 653 Evans, D.A.D., 2003, A fundamental Precambrian-Phanerozoic shift in earth's glacial style?:
654 *Tectonophysics*, v. 375, p. 353-385.
- 655 Farquhar, J., Bao, H., and Thiemens, M., 2000, Atmospheric Influence of Earth's Earliest Sulfur
656 Cycle: *Science*, v. 289, p. 756-758.
- 657 Grotzinger, J.P., and Knoll, A.H., 1995, Anomalous Carbonate Precipitates: Is the Precambrian the
658 Key to the Permian?: *Palaios*, v. 10, p. 578-596.
- 659 Guo, Q., Strauss, H., Kaufman, A.J., Schroder, S., Gutzmer, J., Wing, B., Baker, M.A., Bekker, A.,
660 Jin, Q., Kim, S.-T., and Farquhar, J., 2009, Reconstructing Earth's surface oxidation across
661 the Archaean-Proterozoic transition: *Geology*, v. 37, p. 399-402.
- 662 Halverson, G.P., Hoffman, P.F., Schrag, D.P., and Kaufman, A.J., 2002, A major perturbation of
663 the carbon cycle before the Ghaub glaciation (Neoproterozoic) in Namibia: Prelude to
664 snowball Earth?: *Geochem. Geophys. Geosyst.*, v. 3, p. 1035.
- 665 Hannah, J.L., Bekker, A., Stein, H.J., Markey, R.J., Holland, H.D., 2004. Primitive Os and 2316 Ma
666 age for marine shale: implications for Paleoproterozoic glacial events and the rise of
667 atmospheric oxygen. *Earth and Planetary Science Letters*, v. 225, p. 43-52.
- 668 Haqq-Misra, J.D., Domagal-Goldman, S.D., Kasting, P.J., Kasting, J.F., 2008. A Revised, Hazy
669 Methane Greenhouse for the Archean Earth. *Astrobiology* 8, 1127-1137.

- 670 Hiess, J., Condon, D. J., McLean, N. and Noble, S. R., 2012. $^{238}\text{U}/^{235}\text{U}$ systematics in
671 terrestrial uranium-bearing minerals. *Science*, 335: 1610-1614.
- 672 Hoffman, P.F., 2013. The Great Oxidation Event and a Siderian Snowball Earth: MIF based
673 correlation of Paleoproterozoic glaciations. *Chemical Geology* (in press) DOI:
674 [10.1016/j.chemgeo.2013.04.018](https://doi.org/10.1016/j.chemgeo.2013.04.018)
- 675 Hoffman, P.F., Kaufman, A.J., Halverson, G.P., and Schrag, D.P., 1998, A Neoproterozoic
676 Snowball Earth: *Science*, v. 281, p. 1342-1346.
- 677 Jaffey, A. H., Flynn, K. F., Glendenin, L. E., Bentley, W. C. and Essling, A. M., 1971.
678 Precision measurement of half-lives and specific of ^{235}U and ^{238}U . *Physics Reviews*, C4:
679 1889-1906.
- 680 Kasting, J.F., 2005, Methane and climate during the Precambrian era: *Precambrian Research*, v.
681 137, p. 119-129.
- 682 Kasting, J.F., Zahnle, K.J., and Walker, J.C.G., 1983, Photochemistry of methane in the Earth's
683 early atmosphere: *Precambrian Research*, v. 20, p. 121-148.
- 684 Kaufman, A.J., and Knoll, A.H., 1995, Neoproterozoic variations in the C-isotopic composition of
685 seawater: stratigraphic and biogeochemical implications: *Precambrian Research*, v. 73, p.
686 27-49.
- 687 Kopp, R.E., Kirschvink, J.L., Hilburn, I.A., and Nash, C.Z., 2005, The Paleoproterozoic snowball
688 Earth: A climate disaster triggered by the evolution of oxygenic photosynthesis: *Proceedings*
689 *of the National Academy of Sciences of the United States of America*, v. 102, p. 11131-
690 11136.
- 691 Krogh, T.E., Davis, D.W., and Corfu, F., 1984, Precise U-Pb zircon and baddeleyite ages for the
692 Sudbury area, *in* Pye, E.G., Naldrett, A.J., and Giblin, P.E., eds., *The Geology and Ore*
693 *Deposits of the Sudbury Structure*. Ontario Geological Survey Special Volume, Volume 1,
694 p. 431-446.

- 695 Lowenstein, T.K., Hardie, L.A., Timofeeff, M.N., and Demicco, R.V., 2003, Secular variation in
696 seawater chemistry and the origin of calcium chloride basinal brines: *Geology*, v. 31, p.
697 857–860.
- 698 Marmo, J.S., Ojakangas, R.W., 1984. Lower Proterozoic glaciogenic deposits, eastern Finland.
699 *Geological Society of America Bulletin*, v. 98, p. 1055-1062.
- 700 Martin A.P.; Condon, D.J.; Prave, A.R.; Melezhik, V.A.; Lepland, A.; Fallick, A.E.. 2013
701 Dating the termination of the Palaeoproterozoic Lomagundi-Jatuli carbon isotopic event in
702 the North Transfennoscandian Greenstone Belt. *Precambrian Research*, 224. 160-168.
703 [10.1016/j.precamres.2012.09.010](https://doi.org/10.1016/j.precamres.2012.09.010)
- 704 Matsuhisa, Y., Goldsmith, J.R., and Clayton, R.N., 1979, Oxygen isotopic fractionation in the
705 system quartz-albite-anorthite-water: *Geochimica et Cosmochimica Acta*, v. 43, p. 1131-
706 1140.
- 707 Mattinson, J.M., 2005. Zircon U–Pb chemical abrasion (“CA-TIMS”) method: combined
708 annealing and multi-step partial dissolution analysis for improved
709 precision and accuracy of zircon ages. *Chemical Geology* 220, 47–66.
- 710 Melezhik, V.A., 2006, Multiple causes of Earth's earliest global glaciation: *Terra Nova*, v. 18, p.
711 130-137.
- 712 Melezhik, V. A., 2013, The Imandra/Varzuga Greenstone Belt. In: Melezhik, V.A., Prave, A.R.,
713 Hanski, E.J., Fallick, A.E., Lepland, A., Kump, L.R., Strauss, H. (eds.) *Reading the Archive*
714 *of Earth’s Oxygenation. Volume 1: The Palaeoproterozoic of Fennoscandia as Context for*
715 *the Fennoscandian Arctic Russia - Drilling Early Earth Project. Series: Frontiers in Earth*
716 *Sciences. Springer, Heidelberg, p. 249-287.*
- 717 Melezhik, V.A., Young, G.M., Eriksson, P.G., Altermann, W., Kump, L.R., Lepland, A., 2013a.
718 Huronian-age glaciations. In: Melezhik, V.A., Kump, L.R., Fallick, A.E., Strauss, H.,
719 Hanski, E.J., Prave, A.R., Lepland, A., (eds.) *Reading the Archive of Earth’s Oxygenation.*

- 720 Volume 3: Global Events and the Fennoscandian Arctic Russia - Drilling Early Earth
721 Project. Series: Frontiers in Earth Sciences. Springer, Heidelberg, p. 1059-1109.
- 722 Melezhik, V.A., Hanski, E.J., Prave, A.R., Lepland, A., Romashkin, A.E., Rychanchik, D.V.,
723 Brasier, A.T., Fallick, A.E., Luo, Zh-Y., Sharkov, E.V., Bogina, M.M., 2013b. Polisarka
724 Sedimentary Formation: FAR-DEEP Hole 3A. In: Melezhik, V.A., Prave, A.R., Fallick,
725 A.E., Hanski, E.J., Lepland, A., Kump, L.R., Strauss, H. (eds.), 2013. Reading the Archive
726 of Earth's Oxygenation. Volume 2: The Core Archive of the Fennoscandian Arctic Russia -
727 Drilling Early Earth Project. Series: Frontiers in Earth Sciences. Springer, Heidelberg, p.
728 530-550.
- 729 Mertanen, S., Halls, H. C., Vuollo, J. I., Pesonen, L. J., and Stepanov, V. S., 1999, Paleomagnetism
730 of 2.44 Ga mafic dykes in Russian Karelia, eastern Fennoscandian Shield: implications
731 for continental reconstructions. *Precambrian Research*, v. 98, no. 3-4, p. 197-221.
- 732 Müller, S. G., Krapez, B., Barley, M. E. and Fletcher, I. R., 2005. Giant iron-ore deposits of
733 the Hamersley Province related to the breakup of Paleoproterozoic Australia: new insights
734 from in situ SHRIMP dating of baddeleyite from mafic intrusions. *Geology*, 33: 577-580.
- 735 Negrutsa, V.Z., 1984. Early Proterozoic Stages of Evolution of the Eastern Baltic Shield. Nedra,
736 Leningrad, 270 pp. (in Russian).
- 737 Nelson, D. R., Trendall, A. F. and Altermann, W., 1999. Chronological correlations between
738 the Pilbara and Kaapvaal cratons. *Precambrian Research*, 97: 165-189.
- 739 Papineau, D., Mojzsis, S.J., Coath, C.D., Karhu, J.A., and McKeegan, K.D., 2005, Multiple sulfur
740 isotopes of sulfides from sediments in the aftermath of Paleoproterozoic glaciations:
741 *Geochimica et Cosmochimica Acta*, v. 69, p. 5033-5060.
- 742 Papineau, D., Mojzsis, S.J., and Schmitt, A.K., 2007, Multiple sulfur isotopes from
743 Paleoproterozoic Huronian interglacial sediments and the rise of atmospheric oxygen: Earth
744 and Planetary Science Letters, v. 255, p. 188-212.

- 745 Pavlov, A.A., Hurtgen, M.T., Kasting, J.F., and Arthur, M.A., 2003, Methane-rich Proterozoic
746 atmosphere?: *Geology*, v. 31, p. 87-90.
- 747 Pavlov, A.A., Kasting, J.F., Brown, L.L., Rages, K.A., and Freedman, R., 2000, Greenhouse
748 warming by CH₄ in the atmosphere of early Earth: *J. Geophys. Res.*, v. 105, p. 11981-
749 11990.
- 750 Rosenbaum, J. M., Sheppard, S.M.F., 1986. An isotopic study of siderites, dolomites and ankerites
751 at high temperatures. *Geochimica et Cosmochimica Acta*, v. 50, p. 1147-1159.
- 752 Ravishankara, A.R., 1988, Kinetics of radical reactions in the atmospheric oxidation of CH₄:
753 *Annual Review of Physical Chemistry*, v. 39, p. 367-394.
- 754 Reuschel, M., Strauss, H., Lepland, A., Melezhik, V.A., Cartigny, P., and Kaufman, A.J., 2009,
755 Multiple sulfur isotope measurements from the 2.44 Ga Seidorechka Sedimentary
756 Formation. *Geochimica et Cosmochimica Acta*, v. 73, p. A1091.
- 757 Schidlowski M, Eichmann R, Junge CE (1975) Precambrian sedimentary carbonates: carbon and
758 oxygen isotope geochemistry and implications for the terrestrial oxygen budget.
759 *Precambrian Research*, v. 2, p. 1–69.
- 760 Schlanger, S.O., 1988. Strontium storage and release during deposition and diagenesis of
761 marine carbonates related to sea-level variations., in: Lerman, A., Meybeck, M. (Eds.),
762 *Physical and Chemical Weathering in Geochemical Cycles*. Kluwer, pp. 323-340.
- 763 Scoates, J. S. and Friedman, R. M., 2008. Precise age of the platiniferous Merensky Reef,
764 Bushveld Complex, South Africa, by the U-Pb zircon chemical abrasion ID-TIMS
765 technique. *Economic Geology and the Bulletin of the Society of Economic Geologists*, 103:
766 465-471.
- 767 Steuber, T., Veizer, A., 2002. Phanerozoic record of plate tectonic control of seawater
768 chemistry and carbonate sedimentation. *Geology* 30, 1123-1126.

- 769 Swanson-Hysell, N.L., Rose, C.V., Calmet, C.C., Halverson, G.P., Hurtgen, M.T., and Maloof,
770 A.C., 2010, Cryogenian Glaciation and the Onset of Carbon-Isotope Decoupling: *Science*, v.
771 328, p. 608-611.
- 772 Vallini, D. A., Cannon, W. F. and Schulz, K. J., 2006. Age constraints for Paleoproterozoic
773 glaciation in the Lake Superior region: detrital zircon and hydrothermal xenotime ages for
774 the Chocolay Group, Marquette Range Supergroup. *Canadian Journal of Earth Sciences*, 43:
775 571-591.
- 776 Veizer, J., 1983. Trace elements and isotopes in sedimentary carbonates. *Reviews in*
777 *Mineralogy* 11, 265-299.
- 778 Veizer, J., Clayton, R. N., and Hinton, R. W., 1992, *Geochemistry of Precambrian carbonates: IV.*
779 *Early Paleoproterozoic (2.25 ± 0.25 ga) seawater: Geochimica et Cosmochimica Acta*, v.
780 56, no. 3, p. 875-885.
- 781 Vrevsky, A.B., Bogomolov, E.S., Zinger, T.F., and Sergeev, S.A., 2010, Polychronic sources and
782 isotopic age of the volcanogenic complex (Arvarech unit) of the Imandra-Varzuga
783 structure, Kola Peninsula. *Doklady (Transactions) of the Russian Academy of Sciences*, v.
784 431, p. 386–389.
- 785 White, J.D.L., Houghton, B.F., 2006. Primary volcanoclastic rocks. *Geology* 34,
786 677–680.
- 787 Young, G. M., 1991, *The geological record of glaciation: relevance to the climatic history of the*
788 *Earth: Geoscience Canada*, v. 18, p. 100-108.
- 789 Young, G.M., Long, D.G.F., Fedo, C.M., and Nesbitt, H.W., 2001, Paleoproterozoic Huronian
790 basin: product of a Wilson cycle punctuated by glaciations and a meteorite impact:
791 *Sedimentary Geology*, v. 141-142, p. 233-254.
- 792
- 793
- 794

795 Figure captions

796

797

798 **Fig. 1** Map showing the location of ICDP FAR-DEEP Hole 3A in Fennoscandian Russia

799

800

801 **Fig. 2** Stratigraphy (based on ICDP FAR-DEEP Database) and stratigraphic context of ICDP FAR-
802 DEEP Hole 3A

803

804 **Fig. 3** Images of Polisarka Sedimentary Formation rocks, mostly from cores of ICDP FAR-DEEP
805 Hole 3A. A) Sheared and flattened limestones (some denoted by arrows) in a diamictite at 114.36m.
806 Note the yellow-discoloured dolomitic alteration rims of some of these clasts: these gave low $\delta^{13}\text{C}$
807 values. B) Layered siltstone-carbonate couplets of possible 'varve-like' origin (178.93m depth). C)
808 Deformed layered siltstone-carbonate rocks showing discontinuous lenses of carbonate (one
809 example arrowed; 190.52m). D) Sheared and folded carbonate-siliciclastic rock, including a
810 ptygmatically folded quartz vein (arrowed; 180.25m). E) Talc-rich rock containing numerous
811 dolostone crystals of secondary origin (dolostone crystals are white spots, one of which is arrowed;
812 212.19m). F) Dropstone from an outcrop of the Polisarka Sedimentary Formation. G) Andesitic
813 dropstones in diamictite (ICDP FAR-DEEP Hole 3A, 101.4 m depth; core width is 5 cm). Coin for
814 scale (A-E) is 20mm diameter. Photographs 3F and 3G reproduced with kind permission of
815 Springer Science+Business Media from Victor A. Melezhik, Grant M. Young, Patrick G. Eriksson,
816 Wladyslaw Altermann, Lee R. Kump, and Aivo Lepland (2013) 7.2 Huronian-Age Glaciation. In:
817 V.A. Melezhik, L.R. Kump, A.E. Fallick, H. Strauss, E.J. Hanski, A.R. Prave, A. Lepland (eds.),
818 Reading the Archive of Earth's Oxygenation, Volume 3: Global Events and the Fennoscandian
819 Arctic Russia - Drilling Early Earth Project, pp. 1059-1109. Copyright Springer Science+Business
820 Media 2013.

821

822 **Fig. 4.** Thin-sections of carbonate rocks in ICDP FAR-DEEP Hole 3A. A) Relatively homogenous
823 carbonate rock from 128.35m as seen in cross-polarised light. B) Carbonate rock from
824 182.44m, in cross-polarised light. Note the quartz patches between some of the carbonate
825 crystals (arrowed). C) Carbonate rock with layers of talc (arrowed) from 201.14m in cross-
826 polarised light. D) A layer of talc (brown crenulated mineral) overgrown with a dolomite
827 rhomb (arrowed) (212.19m). E) A dolomite rhomb that has overgrown talc within the
828 peridotite body (147.23m). F) A carbonate rhomb from a carbonatised komatiite at 81.69m.

829

830

831

832 **Fig. 5** The clastic dolostone found at 126.97 m depth in ICDP FAR-DEEP Hole 3A. A) Hand-
833 specimen, stained with Alizarin Red S to distinguish calcite (red-stained layers) from
834 dolomite (unstained). B) Thin-section showing a dolomitic clast under cross-polarised light.
835 Note that quartz grains surround the dolostone clast in the centre. C) Same dolomitic clast
836 viewed in plane polarised light.

837

838

839 **Fig. 6.** Carbonate rock geochemistry, including carbon isotopes, oxygen isotopes, and Mg/Ca ratios.
840 For symbols see the legend and Fig. 2. Note that the data inside the red box belong to the
841 carbonate unit between the peridotite and diamictite. Two excursions to low $\delta^{13}\text{C}$ values are
842 seen as the base of the diamictite is approached. Secondary carbonate within the peridotite
843 body also gives low $\delta^{13}\text{C}$ values. The second excursion at 126.97m is linked to resedimented
844 dolostone clasts. Secondary calcite layers in that same area give higher $\delta^{13}\text{C}$ values. Mg/Ca
845 ratios correlate strongly with $\delta^{13}\text{C}$ in the area of the excursions. Oxygen isotope values are
846 invariably low, and trends seem to reflect carbonate Mg content.

847

848

849 **Fig. 7** Photograph of the rocks between 128.47 m and 124.75 m depth in ICDP FAR-DEEP Hole

850 3A. Note that this section starts with laminated calcites, and includes low $\delta^{13}\text{C}$

851 allochthonous dolostone clasts. Note also the quartz veins, around which the carbonates also

852 have low $\delta^{13}\text{C}$ values.

853

854

855 **Fig. 8** Carbonate $\delta^{13}\text{C}$ (bulk rock samples) and Mn/Sr ratios (for the same bulk-rock samples). For

856 stratigraphic symbols see Fig. 2. Mn/Sr ratios shown in yellow were determined by ICP-

857 AES and those in pink were determined by XRF. Note that the data within the red box

858 belong to the carbonate unit between the peridotite and diamictite.

859

860 **Fig. 9** A cross-plot of carbonate $\delta^{18}\text{O}$ (x-axis) vs $\delta^{13}\text{C}$ (y-axis). For symbols see the legend. Oxygen

861 isotope values are not corrected for their Mg content (data presented as if samples were all

862 calcite). Their oxygen isotope values are relatively invariant, hence the trend mostly runs

863 parallel to the Y axis. A possible mixing-line trend (black line) likely reflects mixing

864 between ‘calcite’ and ‘dolomite’ end-members. See text for discussion.

865

866

867 **Fig. 10** $^{207}\text{Pb}/^{206}\text{Pb}$ histogram plots of LA-ICPMS data for samples targeted for chronology and the

868 location of samples from drill core 3A. Sample Ru1310 was collected in the field at 67°

869 11.984 N and 35° 46.361 E. Lithological column is based on FAR-DEEP Database.

870

871 **Fig. 11** Petrography of drill core sample 3A 20.01 m (ash from which zircons were obtained). A)
872 Hand specimen. L = lithic. P = pumice. C = crystal. B) Thin section. P = pumice. Qtz =
873 quartz (volcanic).

874

875 **Fig. 12:** Conventional concordia plot for zircons analysed from sample 3A 20.01 m.

876

877 **Table 1:** U-Th-Pb data for zircons analysed from sample ICDP FAR-DEEP Hole 3A 20.01 m

878

879 Captions for supplementary tables and figure are given in the file 'supplementary information'

880

881

882

883

884

885

886

887

Research highlights:

ICDP FAR-DEEP Hole 3A targeted Palaeoproterozoic diamictites of the Polisarka

Sedimentary Formation of Russian Fennoscandia ► Zircon U-Pb dating of a tuff above the

diamictites yielded an interpreted minimum age of 2434 Ma for the diamictites ► This

constrains the onset of the Palaeoproterozoic glaciation in Fennoscandia to between ca. 2430

and ca. 2440 Ma ► carbonate $\delta^{13}\text{C}$ analyses of carbonate rocks below the diamictites

revealed two excursions to ca. -5‰ ► the origins of these excursions are carefully

considered

Accepted Manuscript

Fraction	Radiogenic Isotope Ratios										Isotopic Ages								
	Th/U (b)	$^{206}\text{Pb}^*/^{206}\text{Pb}$ x10 ⁻¹³ mol (c)	mol % $^{206}\text{Pb}^*$ (c)	$\frac{\text{Pb}^*}{\text{Pb}_c}$ (c)	Pb _c (pg) (c)	$\frac{^{206}\text{Pb}}{^{204}\text{Pb}}$ (d)	$\frac{^{206}\text{Pb}}{^{206}\text{Pb}}$ (e)	$\frac{^{207}\text{Pb}}{^{206}\text{Pb}}$ (e)	% err (f)	$\frac{^{207}\text{Pb}}{^{235}\text{U}}$ (e)	% err (f)	$\frac{^{206}\text{Pb}}{^{238}\text{U}}$ (e)	% err (f)	$\frac{^{207}\text{Pb}}{^{235}\text{U}}$ (g)	± (f)	$\frac{^{206}\text{Pb}}{^{238}\text{U}}$ (g)	± (f)		
z2	0.787	4.1196	99.61%	86	1.37	43.97	0.224	0.156904	0.089	9.688111	0.293	0.447821	0.254	2422.5	1.5	2405.6	2.7	2385.6	5.1
z3	0.486	12.0116	99.88%	280	1.17	15203	0.135	0.189230	0.080	13.728777	0.173	0.526188	0.103	2735.4	1.3	2731.2	1.6	2725.4	2.3
z4	0.472	1.6033	99.33%	49	0.90	2718	0.131	0.189681	0.096	13.794564	0.337	0.527453	0.303	2739.3	1.6	2735.7	3.2	2730.8	6.7
z6	0.331	1.4206	98.87%	27	1.39	1499	0.101	0.198730	0.222	12.805982	0.440	0.467355	0.374	2815.7	3.6	2665.5	4.1	2472.0	7.7
z7	1.040	7.5733	99.54%	72	3.15	3346	0.296	0.157161	0.090	9.714832	0.177	0.448323	0.098	2425.3	1.5	2408.1	1.6	2387.8	2.0
z8	0.968	3.8219	98.99%	32	3.49	1523	0.275	0.155794	0.099	9.582447	0.224	0.446091	0.158	2410.5	1.7	2395.5	2.1	2377.9	3.1
z9	0.938	6.6041	99.42%	57	3.44	2664	0.266	0.158101	0.093	9.829474	0.191	0.450913	0.117	2435.4	1.6	2418.9	1.8	2399.4	2.3
z11	0.939	1.2339	98.17%	18	2.02	882	0.264	0.157854	0.123	9.969447	0.332	0.458051	0.275	2432.8	2.1	2432.0	3.1	2431.0	5.6
z12	0.461	7.0665	99.46%	54	3.47	2820	0.130	0.158146	0.089	9.967708	0.182	0.457125	0.105	2435.9	1.5	2431.8	1.7	2426.9	2.1
z13	0.512	9.3420	99.77%	140	1.84	7239	0.141	0.198694	0.085	15.005791	0.186	0.547739	0.120	2815.5	1.4	2815.6	1.8	2815.8	2.7
z31	0.354	1.7701	94.52%	5	9.42	268	0.100	0.194517	0.216	13.892947	0.736	0.518008	0.689	2780.7	3.5	2742.4	7.0	2690.8	15.2
z39	0.251	0.2721	91.03%	3	2.37	177	0.073	0.169418	0.858	10.483936	1.854	0.448811	1.567	2551.8	14.4	2478.5	17.2	2390.0	31.3
z43	0.146	1.2562	99.38%	49	0.65	2955	0.040	0.188104	0.096	13.695541	0.352	0.528057	0.318	2725.6	1.6	2728.9	3.3	2733.3	7.1
z44	0.581	0.5824	98.17%	18	0.90	994	0.159	0.194837	0.153	14.615500	0.689	0.544053	0.667	2783.4	2.5	2790.5	6.6	2800.5	15.1
z15	0.510	0.5825	93.76%	5	3.49	246	0.139	0.189949	0.230	14.193600	0.734	0.541943	0.691	2741.7	3.8	2762.7	7.0	2791.6	15.7
z23	0.730	2.3370	98.69%	24	2.75	1196	0.202	0.185026	0.102	13.224841	0.529	0.518391	0.504	2698.4	1.7	2695.8	5.0	2692.4	11.1

(a) z1, z2 etc. are labels for fractions composed of single zircon grains or fragments; all fractions annealed and chemically abraded after *Mattinson* [2005].

(b) Model Th/U ratio calculated from radiogenic $^{208}\text{Pb}/^{206}\text{Pb}$ ratio and $^{207}\text{Pb}/^{235}\text{U}$ age.

(c) Pb^* and Pb_c represent radiogenic and common Pb, respectively; mol % $^{206}\text{Pb}^*$ with respect to radiogenic, blank and initial common Pb.

(d) Measured ratio corrected for spike and fractionation only.

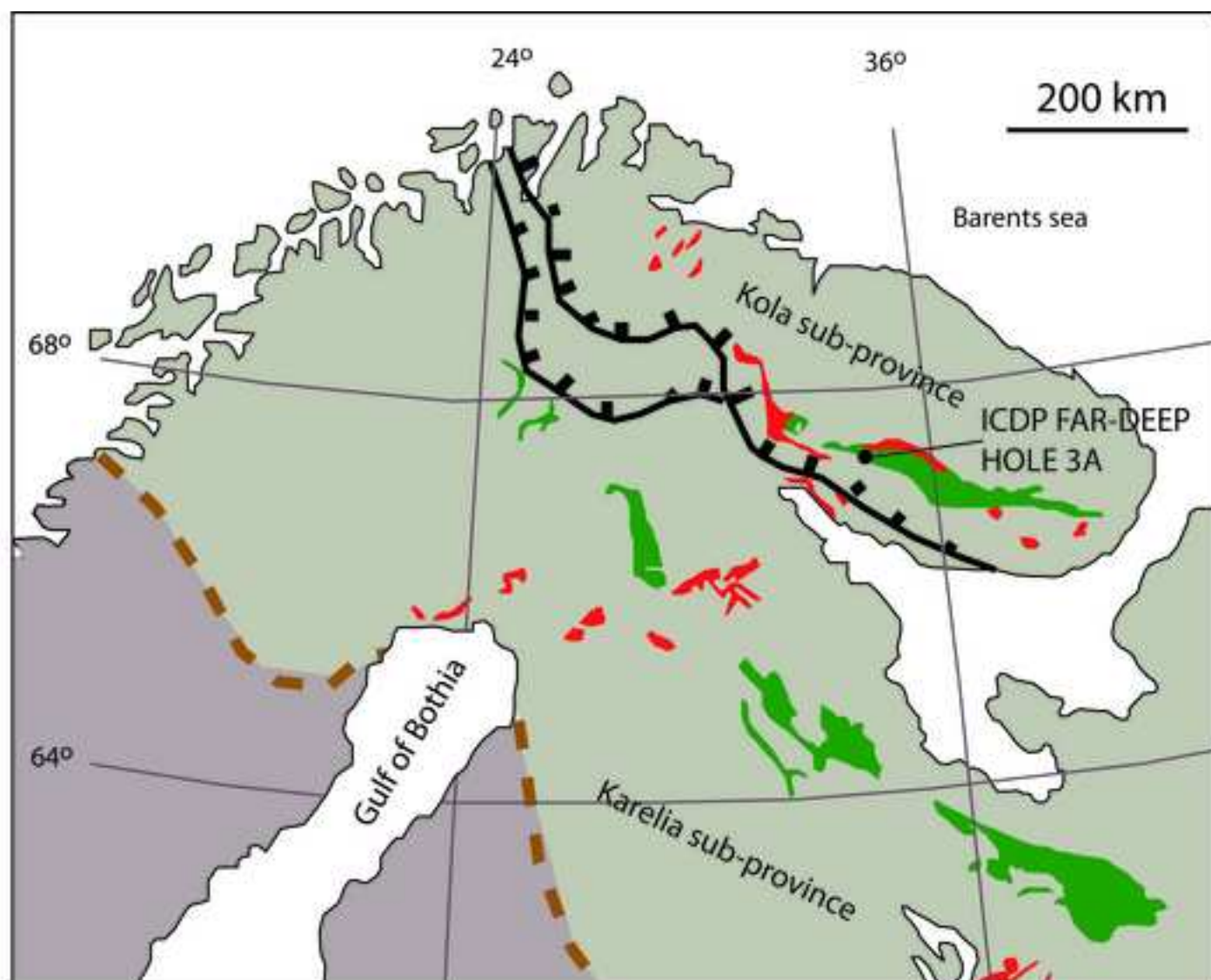
(e) Corrected for fractionation, spike, and common Pb; up to 1 pg of common Pb was assumed to be procedural blank: $^{206}\text{Pb}/^{204}\text{Pb} = 18.20 \pm 0.50\%$; $^{207}\text{Pb}/^{204}\text{Pb} = 15.65 \pm 0.40\%$.


(f) Errors are 2-sigma, propagated using the algorithms of *Schmitz and Schoene* [2007] and *Crowley et al.* [2007].

(g) Calculations are based on the decay constants of *Jaffey et al.* [1971]. $^{206}\text{Pb}/^{238}\text{U}$ and $^{207}\text{Pb}/^{238}\text{U}$ ages corrected for initial disequilibrium in $^{230}\text{Th}/^{238}\text{U}$ using Th/U [magmal] = 4.

$^{206}\text{Pb}/^{238}\text{U}$ dates in bold are those used in the weighted mean zircon date calculation

Table 1: U-Th-Pb data for zircons analysed from sample ICDP FAR-DEEP Hole 3A
20.01 m



 Svecofennian rocks

 Archaean craton

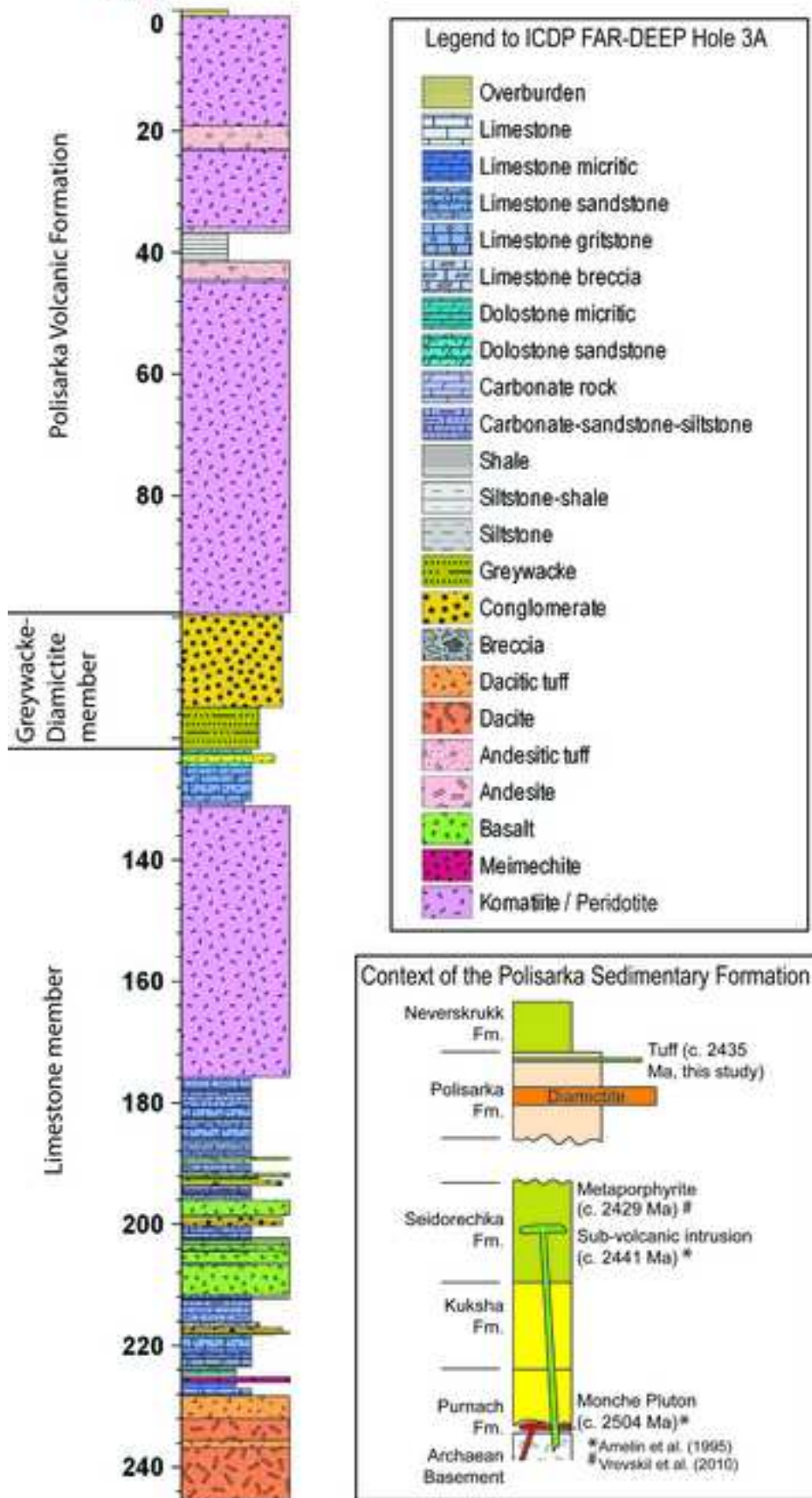
 Sumi flood-basalt

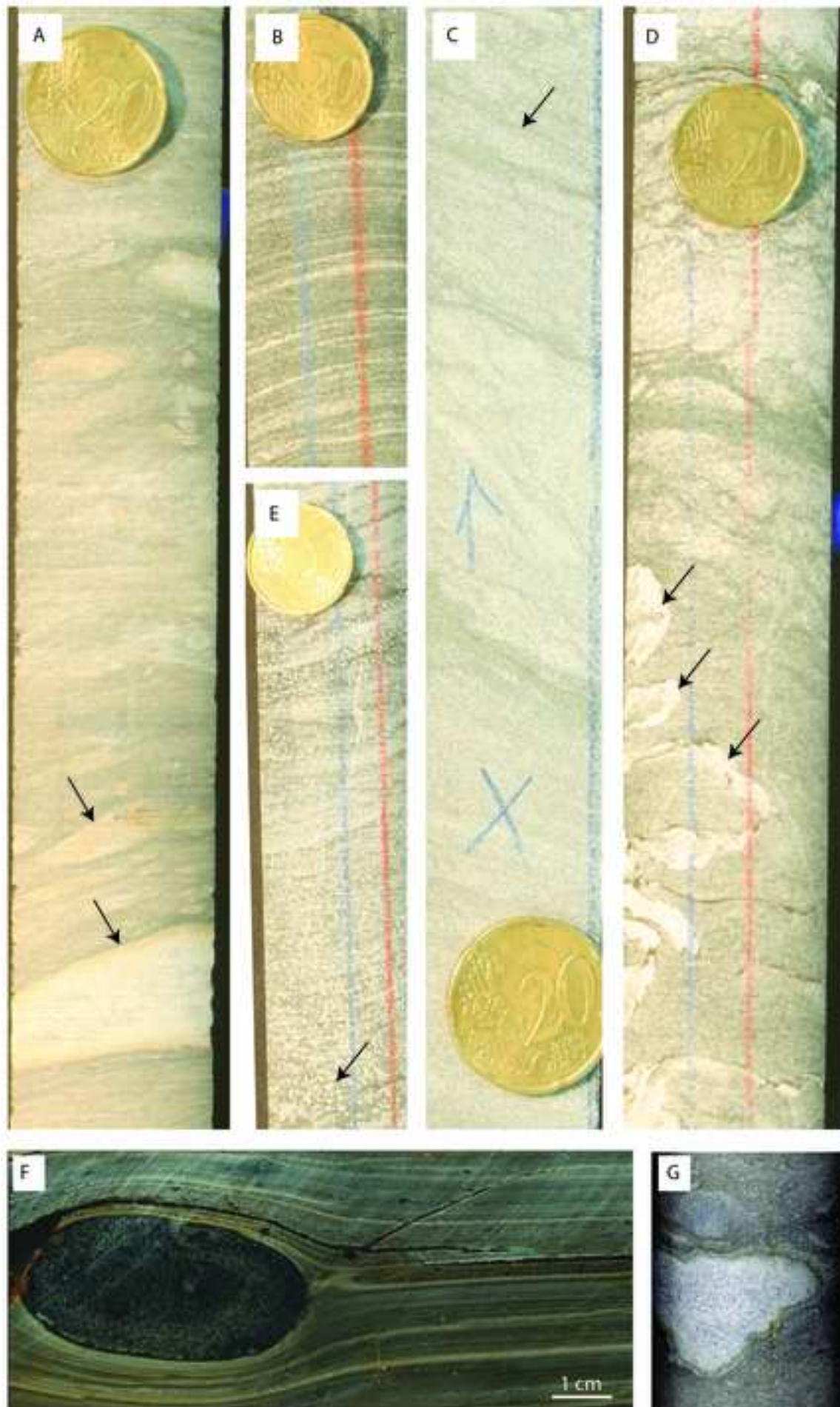
 Layered gabbro-norite

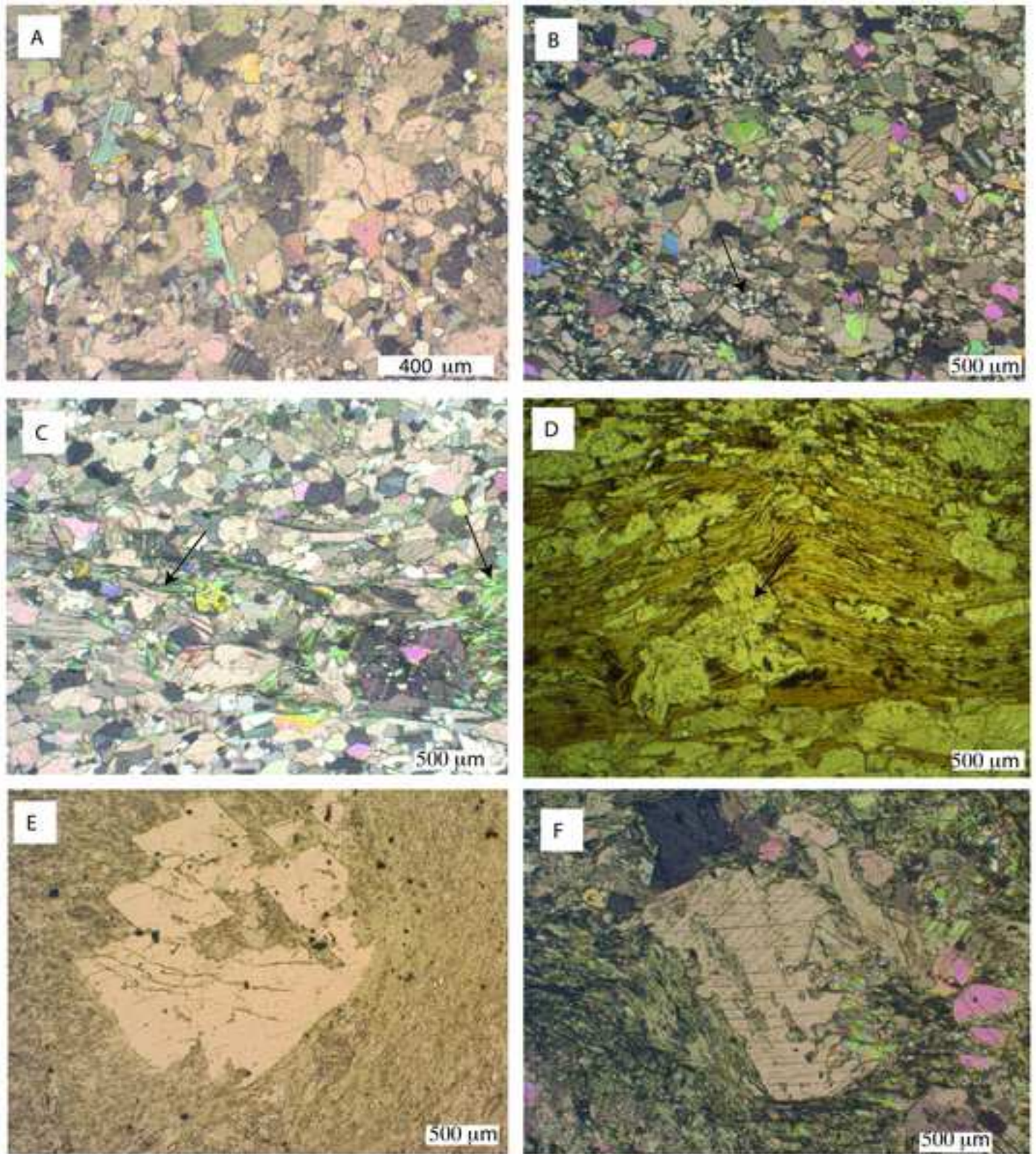
 Lapland - Kola Suture

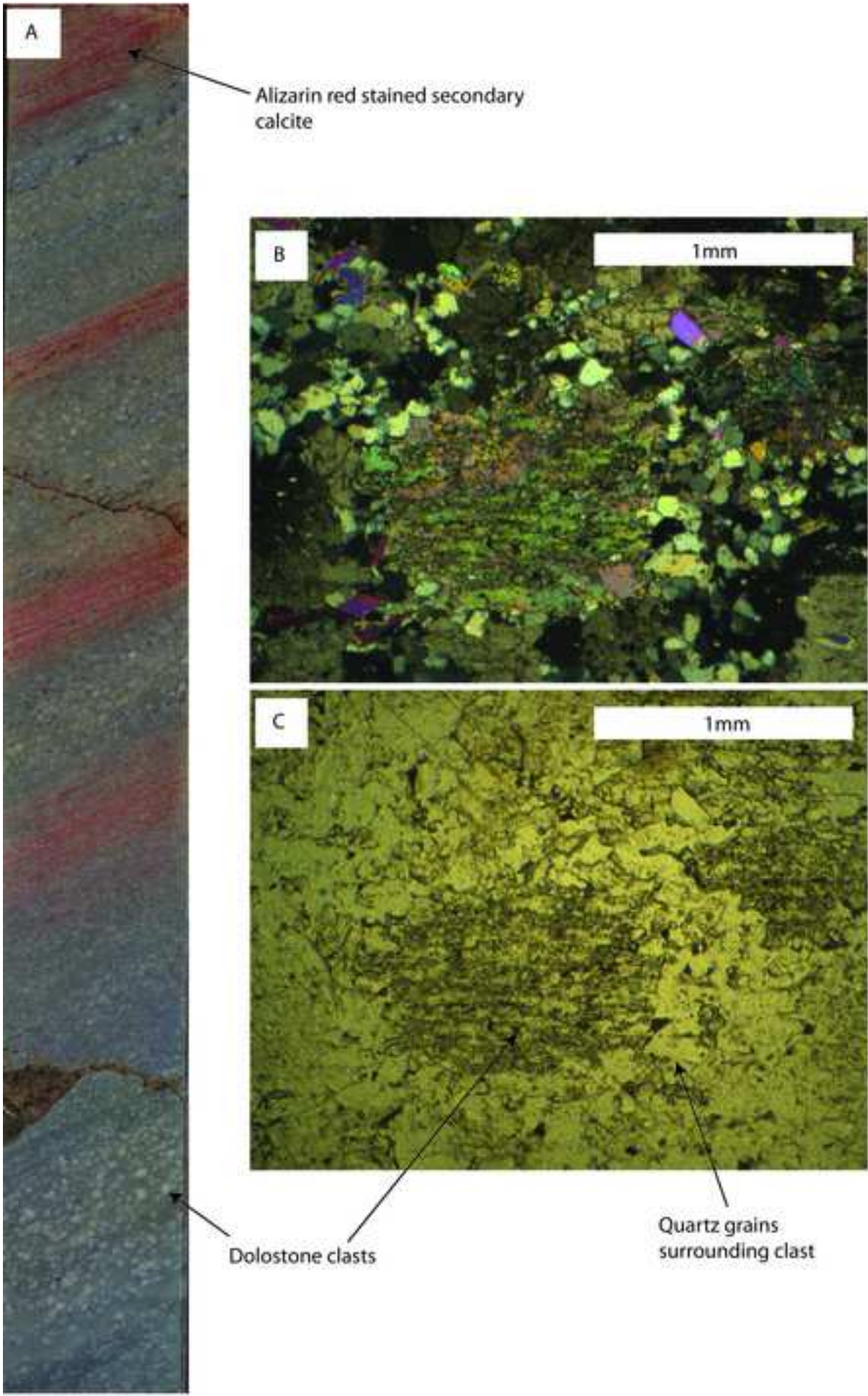


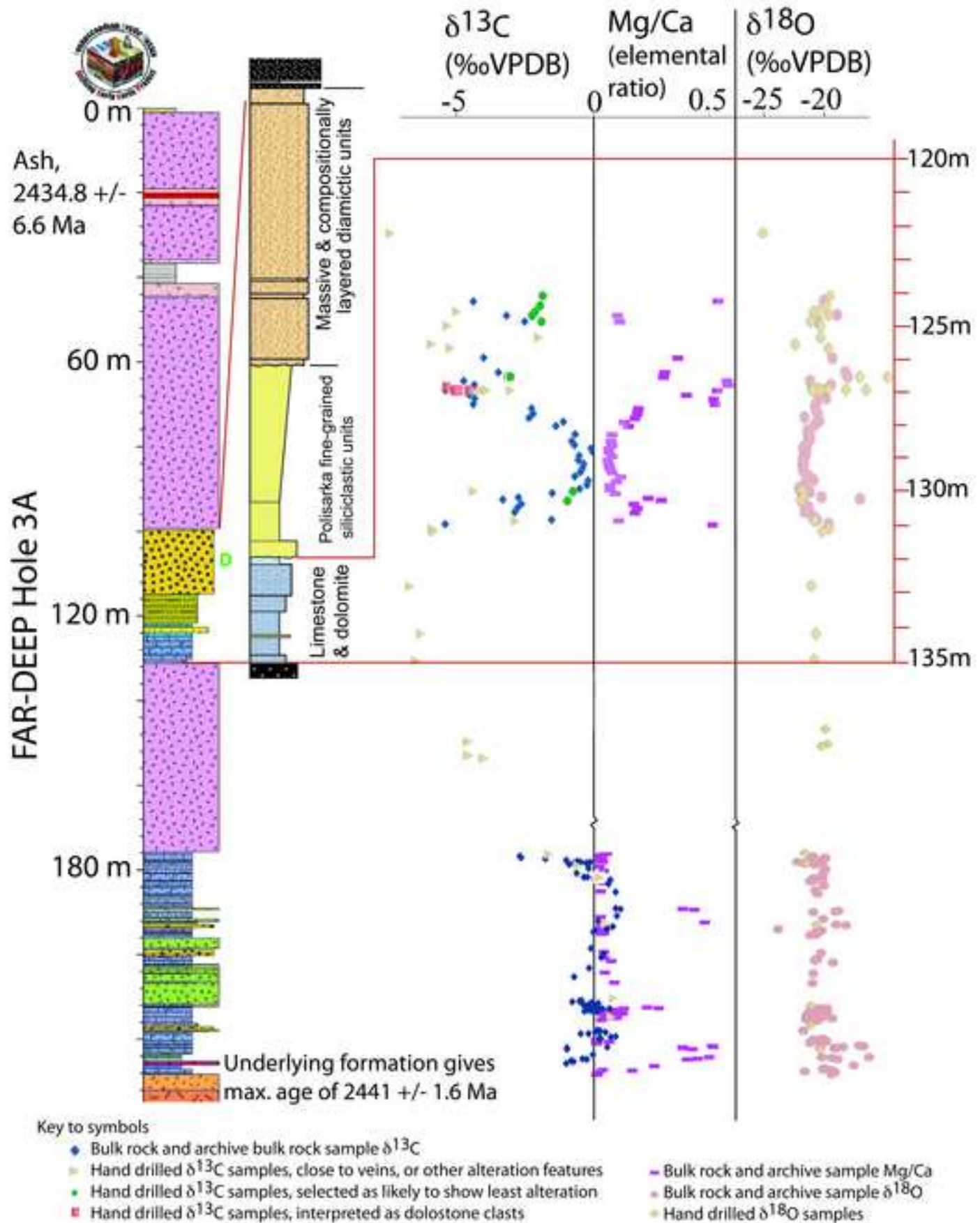
3A

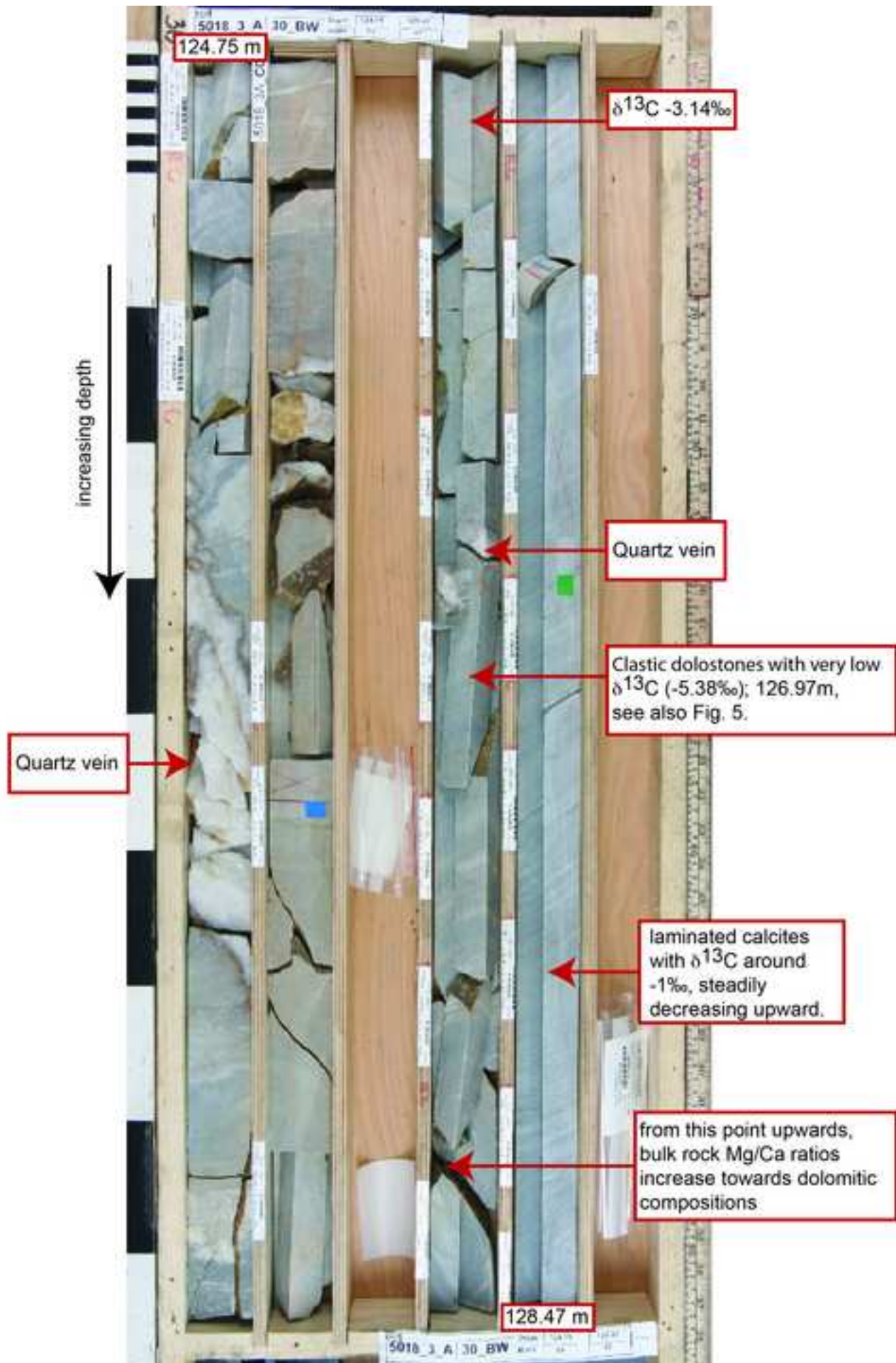


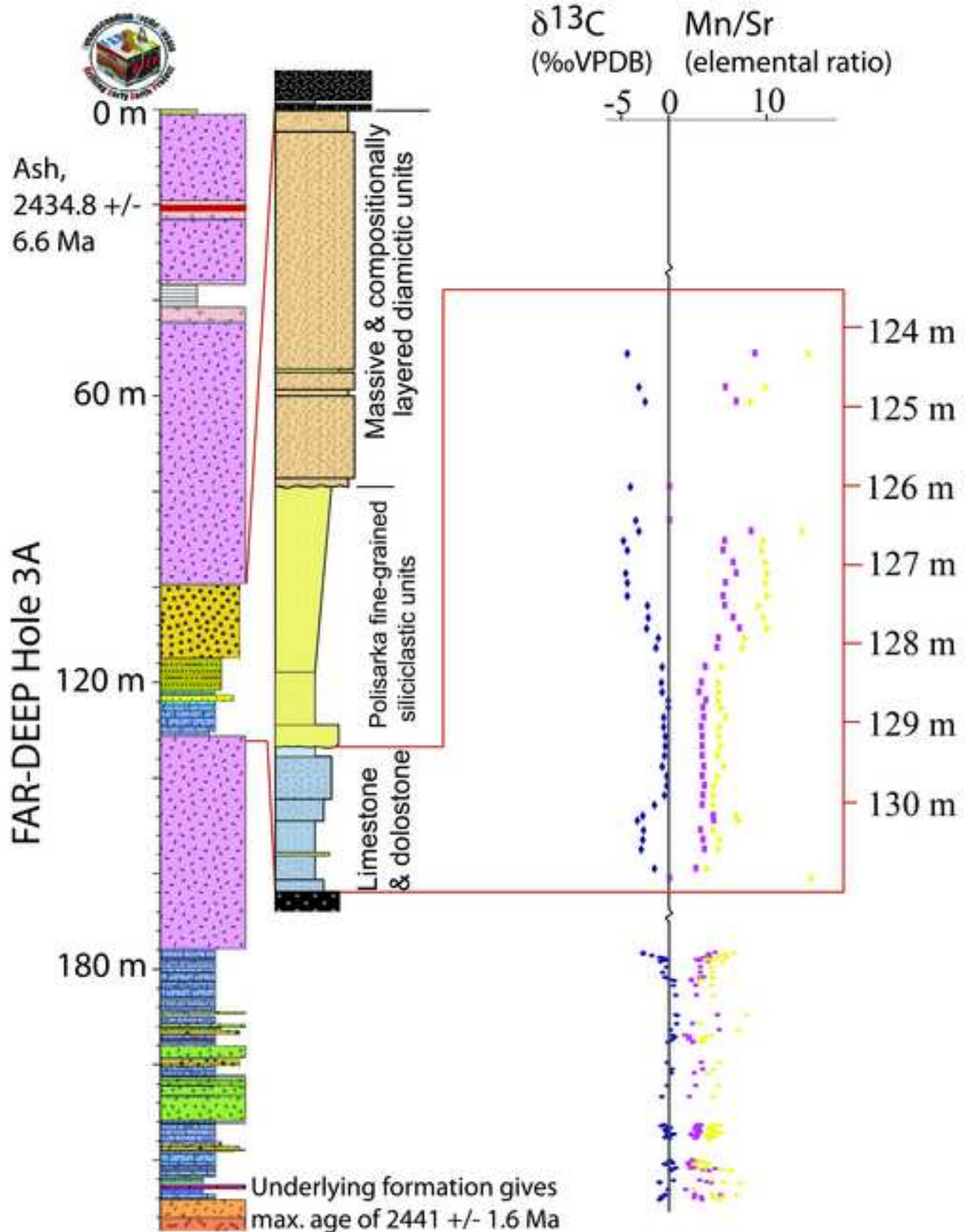




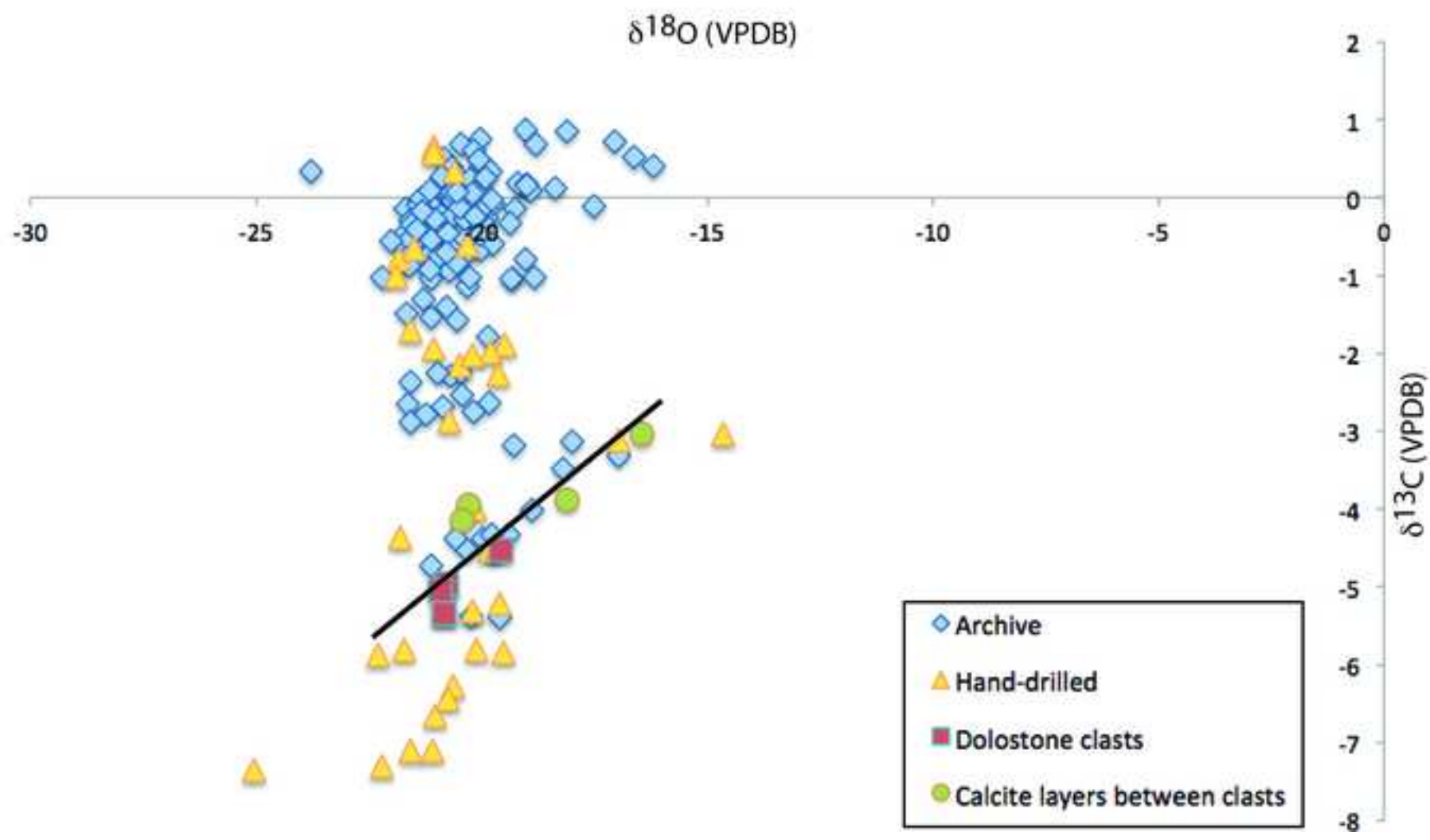


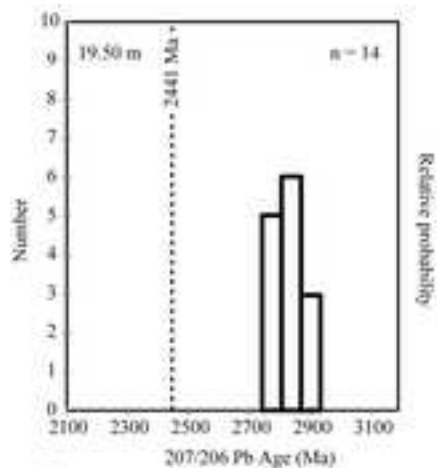




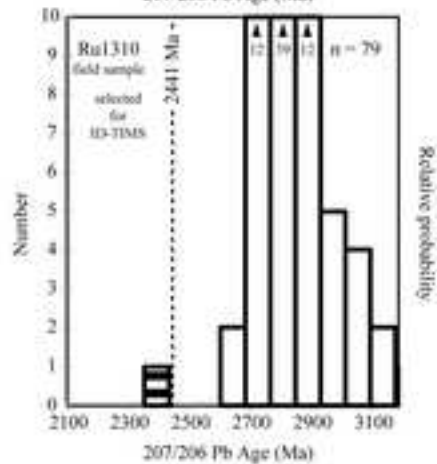
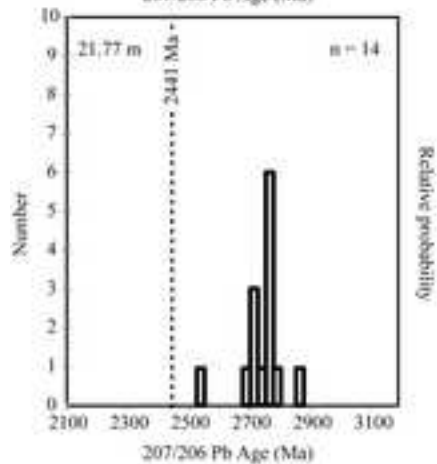
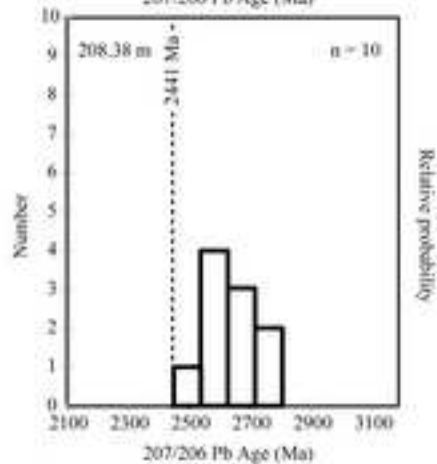
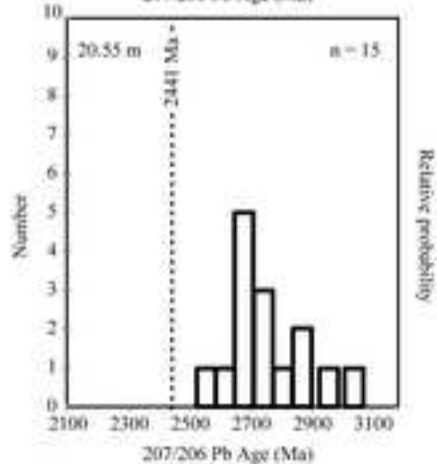
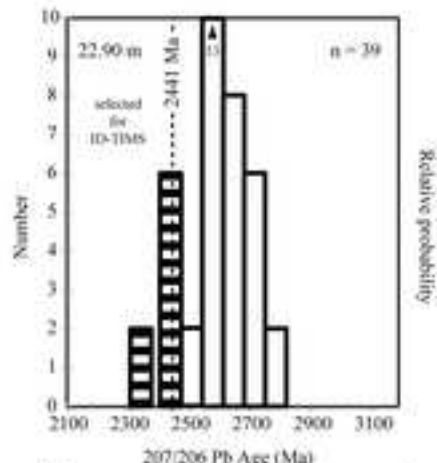
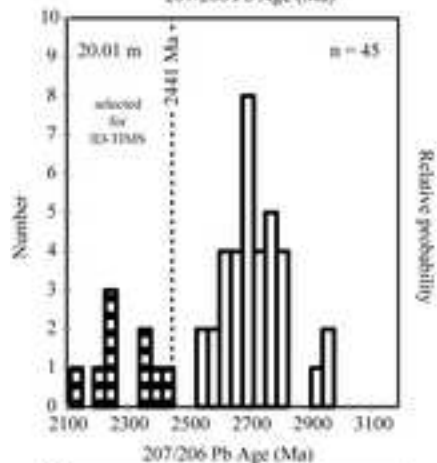


scrip





Sample locality
 Basement = Inheritance
 age > 2441 Ma



Hole 3A

19.5m. 14 zircons. Basement.
 20.1m. 45 zircons. Palaeoproterozoic.
 20.55m. 15 zircons. Basement.
 21.77m. 14 zircons. Basement.
 22.65m. No zircon.
 22.90m. 39 zircons. Basement.

80.40m. No zircon.
 86.16m. No Zircon.
 93.13m. No Zircon.

207.30m. No zircon.
 207.85m. 2 zircons. Basement.
 208.38m. 10 zircons. Basement.

238.23m. No zircons.
 245.76m. No zircons.

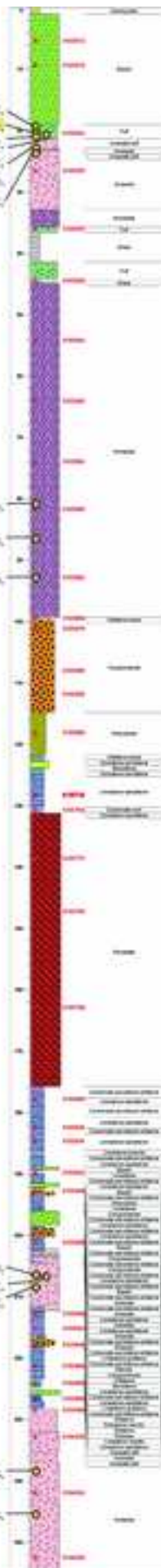


Figure 11

manuscript

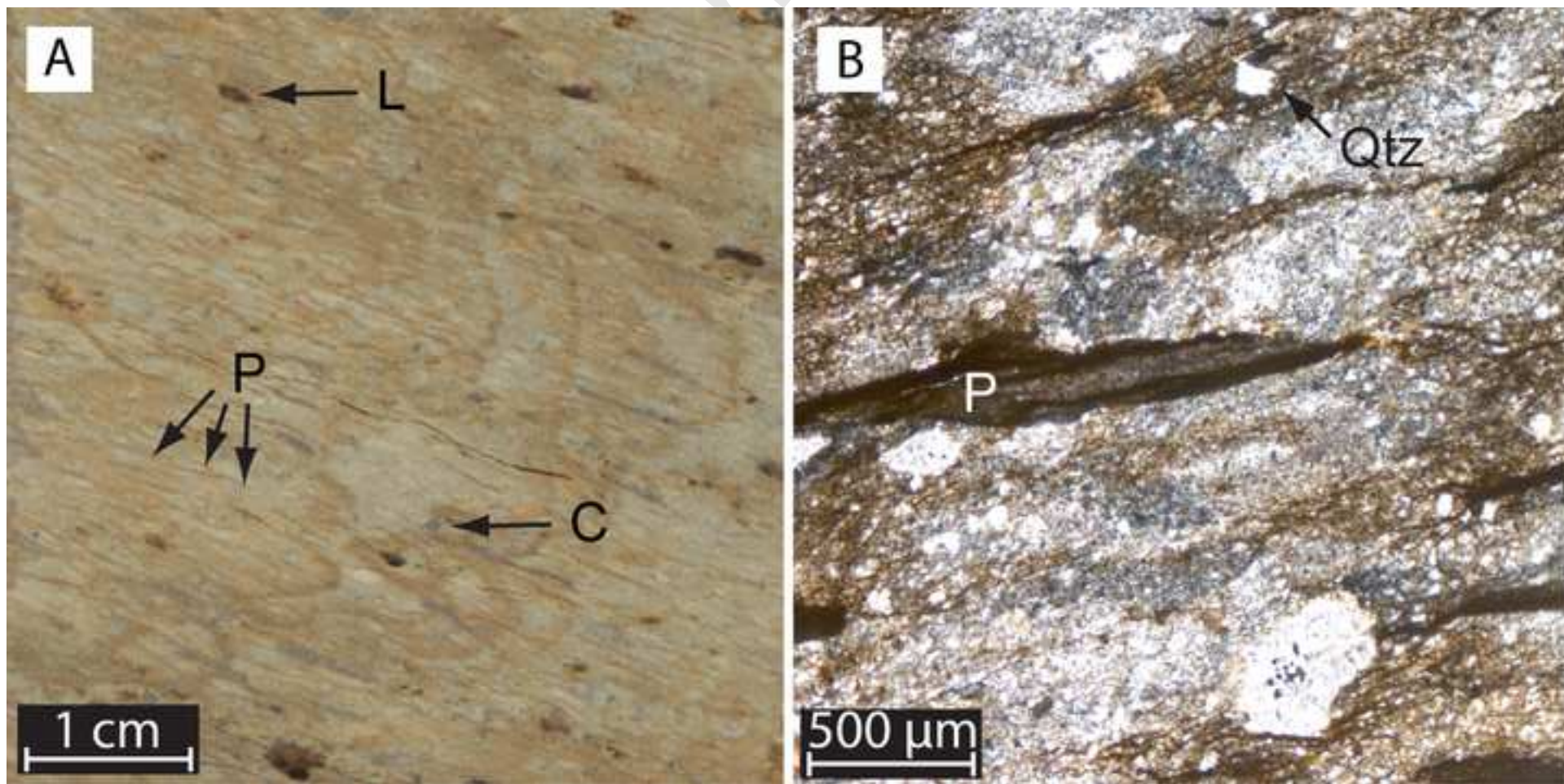


Figure 12

